Probabilistic Constellation Shaping for Optical Fiber Communications

Junho Cho, *Member, IEEE*, and Peter J. Winzer, *Fellow, IEEE, Fellow, OSA*

(Invited Paper)

***Abstract*—We review probabilistic constellation shaping (PCS), which has been a key enabler for several recent record-setting optical fiber communications experiments. PCS provides both fine-grained rate adaptability and energy efficiency (sensitivity) gains. We discuss the reasons for the fundamentally better performance of PCS over other constellation shaping techniques that also achieve rate adaptability, such as time-division hybrid modulation, and examine in detail the impact of sub-optimum shaping and forward error correction (FEC) on PCS systems. As performance metrics for systems with PCS, we compare information-theoretic measures such as mutual information (MI), generalized MI (GMI), and normalized GMI, which enable optimization and quantification of the information rate (IR) that can be achieved by PCS and FEC. We derive the optimal parameters of PCS and FEC that maximize the IR for both ideal and non-ideal PCS and FEC. To avoid plausible pitfalls in practice, we carefully revisit key assumptions that are typically made for ideal PCS and FEC systems.**

***Index Terms*—Modulation, optical fiber communication, probabilistic constellation shaping, quadrature amplitude modulation.**

I. Introduction

IT HAS been known since 1948 when information theory was first established in Shannon's seminal paper [1] that a continuous Gaussian source distribution achieves the capacity of the additive white Gaussian noise (AWGN) channel when ideal forward error correction (FEC) is assumed. Between the late 1980s and the early 1990s, many studies developed discrete modulation techniques to mimic continuous Gaussian signaling, commonly referred to as *constellation shaping* [2]–[6]. Constellation shaping, however, did not find broad applications, except for the V.34 voice band modem over telephone lines that was standardized by the International Telecommunications Union (ITU) in 1994 [7]. While constellation shaping attempts to approach the Shannon limit from a *modulation* perspective, approaching the Shannon limit from a *coding* perspective saw a new wave of substantial progress with the invention of turbo codes in 1993 [8]. The success of turbo codes led to the rediscovery of low-density parity-check (LDPC) codes [9]–[11], which reduced the *coding gap* to the (modulation-constrained) Shannon limit to within tenths of a decibel. Remarkably, capacity-approaching soft-decision (SD) FEC codes have a good structure for low-cost parallel application-specific integrated circuit (ASIC) implementation, and have hence been adopted as a quasi-standard in almost every field of communications [12]–[18]. A tremendous amount of research has been published in the golden era of FEC since 1993, and research on constellation shaping was relatively unpopular except for a small number of isolated papers, e.g., [19]–[25]. This may be partly because the *shaping gain* relative to a square quadrature amplitude modulated (QAM) constellation is fundamentally limited to $\sim$1.53 dB, while the *coding gain* with modern SD FEC codes easily reaches 10 dB at a bit error ratio (BER) of 10^{-15}, and partly because there was no effective method to implement capacity-approaching constellation shaping up until very recently.

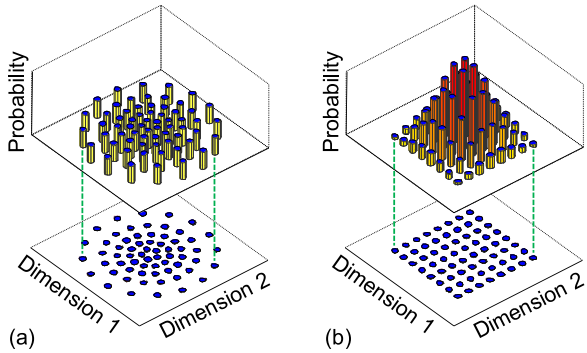

Fig. 1. (a) Geometric and (b) probabilistic constellation shaping.

In the context of optical communications, *geometric constellation shaping (GCS)* in the form of multi-ring constellations was used to estimate the Shannon limit of the nonlinear optical fiber channel [26], and in the form of iterative polar modulation (IPM) to achieve experimental spectral efficiency (SE) records [27], [28]. Using GCS, the *location* of the constellation points in the complex plane is arranged to approximate a Gaussian distribution, cf. Fig. 1(a). However, GCS has some serious practical disadvantages that have prevented its commercialization: *(i)* there is no simple solution to finding locations of the GCS constellation points for arbitrary channel conditions; *(ii)* the irregular constellation points of GCS increase the complexity of coherent digital signal processing (DSP) for robust signal recovery prior to decoding; and *(iii)* the general infeasibility of

Manuscript received December 6, 2018; revised January 9, 2019 and February 7, 2019; accepted February 8, 2019. Date of publication February 12, 2019; date of current version March 28, 2019. *(Corresponding author: Junho Cho.)*

The authors are with Nokia Bell Labs, Holmdel, NJ 07733 USA (e-mail: junho.cho@nokia-bell-labs.com; peter.winzer@nokia-bell-labs.com).

Color versions of one or more of the figures in this paper are available online at http://ieeexplore.ieee.org.

Digital Object Identifier 10.1109/JLT.2019.2898855

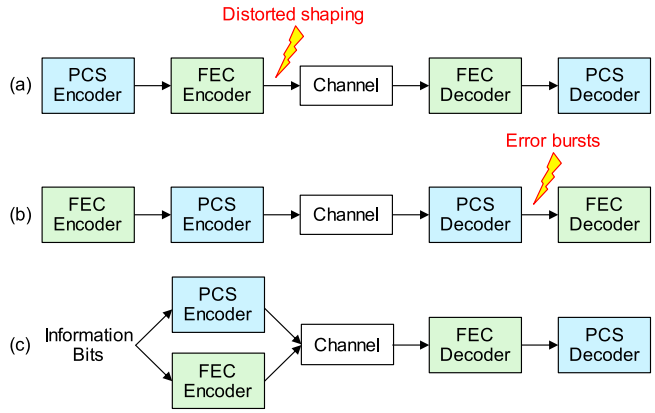

Fig. 2. Architectures for PCS.

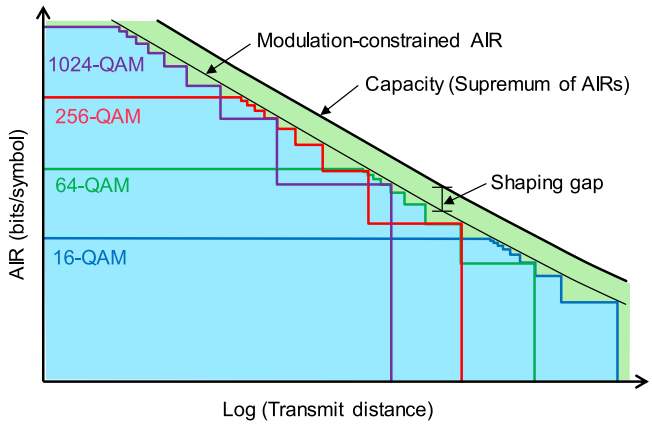

Fig. 3. Schematic illustration of the AIR of the auxiliary AWGN channel modeling an optical fiber channel. Upper solid line: Gaussian signaling (i.e., AWGN capacity), lower solid line: uniform QAMs with arbitrarily rate-adaptable FEC (i.e., modulation-constrained AIR), staircase lines: uniform QAMs with nine different fixed-rate FEC codes (i.e., modulation- and code-constrained AIRs).

Gray mapping increases the complexity of demapping symbols to soft-decision bit metrics.

It is only four years ago that constellation shaping began to attract significant attention, both in research and in rapidly following productization, in the form of *probabilistic constellation shaping (PCS),* which shapes the *probability of occurrence* of the constellation points rather than their locations to approximate Gaussian signaling, as shown in Fig. 1(b). In contrast to GCS, *(i)* it is simple to optimize these probabilities through a single parameter to match any given channel condition, *(ii)* constellation points are placed on the rectilinear grid of a *square QAM template*, which facilitates coherent DSP by robust state-of-the-art square-QAM algorithms, and *(iii)* Gray mapping facilitates symbol demapping for subsequent SD FEC.

Combinations of PCS and GCS have also been studied in the context of optical communications [29], [30], but these have yielded little gain over pure PCS based on square QAM templates, which already approach the Shannon limit to within 0.1 dB in the AWGN channel. Nevertheless, the combination of GCS and PCS to combat channel nonlinearities [31], [32] is not yet a completely resolved problem.

PCS is practically enabled by the *probabilistic amplitude shaping (PAS)* architecture [33], which shows capacity-approaching performance with a practical shaping and coding implementation and elegantly resolves the long-standing problem of PCS in terms of combining shaping and coding, as visualized in Fig. 2: The problem with previously known PCS architectures is that performing *coding after shaping* at the transmitter distorts the shaped symbol distribution, as FEC parity bits are generally not shaped, see Fig. 2(a). On the other hand, performing *coding before shaping* at the transmitter can cause error bursts upon de-shaping erroneously received symbols at the receiver, see Fig. 2(b). The PAS architecture elegantly circumvents this problem by optimally intertwining shaping and coding in a capacity-approaching and efficiently implementable way, cf. Fig. 2(c). Coding and shaping are decoupled through a parallel transmitter architecture (as reviewed in Section II-A.) such that their independent optimization leads to jointly optimal performance. This greatly simplifies the implementation of encoder and decoder by allowing the use of off-the-shelf modern SD FEC codes, with minimum to no specific tailoring for the use in a PCS application.

PCS based on the PAS architecture in optical communications was first demonstrated by full-field simulations [34] and transmission experiments [35] in 2015. Record SEs using PCS were then demonstrated across a wide range of transmission distances from 500 km to 4,000 km [36], and a capacity of 65 Tb/s was demonstrated at a record SE using PCS, exploiting C and L bands over 6,600 km in a laboratory experiment [37]. The first field trial over a trans-oceanic submarine cable using PCS achieved a record SE over 5,500 km and 11,000 km [38]. Over a short distance of 50 km, a record SE of 17.3 b/s/Hz was demonstrated using PCS on a 10-subcarrier superchannel [39], [40]. The first commercial transponder using PCS was recently announced [41]. The first real-time experimental demonstration of PCS was reported in [42]. The numerous milestones that have been achieved in only 4 years and the rapid adoption of PCS in the commercial sector bear testimony to the significance of PCS in improving the performance of optical fiber communications.

II. Benefits of PCS in Optical Transmission

A. Fiber Channel Capacity and Achievable Information Rates

The trade-off between the *achievable information rate (AIR)* and the transmission distance in a fiber-optic transmission system is illustrated in Fig. 3; as the figure merely visualizes general trade-offs, the exact axis labels that vary depending on the underlying system assumptions are omitted. While the nonlinear fiber channel is a non-AWGN channel with memory, whose general capacity has been estimated but is not exactly known [26], [43], it can under certain assumptions be *accurately modeled* as a memoryless AWGN channel [26], [44]–[46]. The AIR for this *auxiliary* AWGN channel can then be maximized over all possible input distributions, assuming ideal FEC coding with infinite code length and unlimited decoder complexity, leading to a capacity estimate of the fiber channel as represented by its auxiliary AWGN channel. The capacity of the auxiliary

AWGN channel, however, does not represent the fundamental fiber channel capacity, but rather a lower bound of it, in the sense that a higher AIR may be obtained if one could further exploit intra- and inter-channel nonlinear interference to enhance the signal-to-noise ratio (SNR). The largest recovered SNR of a fiber channel depends on the network scenario and on assumptions about what information is and is not known to the various transponders within the network. This leads to a variety of capacity estimates for the optical fiber channel [26], [46]. Regardless of the sophistication of the optical fiber channel model, it is a general observation that capacity is maximized by a certain optical signal power. Furthermore, as both optical amplifier noise [26] and nonlinear interference noise (NLIN) at optimized optical channel powers [44]–[46] are, either exactly or to an excellent approximation for Gaussian signaling, linearly proportional to the transmission reach, the channel capacity decreases logarithmically with transmission distance in the high SNR regime, as illustrated by the upper solid line in Fig. 3 [46]. Achieving the auxiliary AWGN channel capacity implies, at each transmission distance, the use of the optimally chosen variance of a Gaussian-shaped modulation as well as optimal FEC performance at an optimally chosen code rate $R_c \in (0, 1]$; hence, attaining the capacity involves the *continuous adaptation* of both modulation *and* FEC code rate. If we restrict ourselves to uniform square QAM constellations, the *modulation-constrained* AIR is decreased to below the modulation-unconstrained AIR (i.e., the capacity of the auxiliary channel), as indicated by the lower solid line in Fig. 3, suffering a loss called the *shaping gap* due to the non-Gaussianity of the signal. In principle, the QAM-constrained AIR can be reached by optimizing the FEC code rate for each transmission distance with uniform square QAM formats. However, in practical ASIC implementations, only a few code rates may be available, which lets the AIR decrease in the form of a staircase function versus distance, as shown for nine different FEC rates $R_c = 1/2, 2/3, \ldots, 9/10$ in Fig. 3. Despite these many FEC rates, there is still a significant gap to the optimal AIR, as well as a step-like rate/reach trade-off. Compared to uniform QAM, PCS achieves *both* an arbitrarily fine rate/reach trade-off, even for a *single* FEC code rate, *and* bridges the shaping gap to closely approach ultimate performance. These two distinct benefits of PCS will be discussed in the context of contending techniques in the subsequent Sections II-B and II-C.

B. Rate Adaptation

1) Uniform Square QAM With Multi-Rate FEC: In order to perform rate adaptation by FEC alone, as discussed along with Fig. 3, the most common way in communication standards is to use a small family of base matrices for LDPC coding, which are highly optimized using, e.g., density evolution [11] or extrinsic information transfer (EXIT) chart analyses [47], to approach the (modulation-constrained) AIR. Every matrix in the family of FEC codes is made to be a sub-matrix of a larger matrix to establish a good structure for ASIC implementation. The base matrices are then *lifted* by replacing each non-zero element with a $z \times z$ circulant matrix such that larger matrices can be derived for actual LDPC codes. This construction limits the derived code

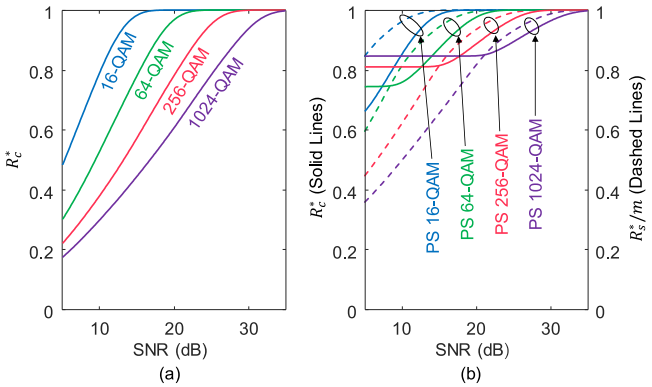

Fig. 4. (a) Optimal code rate R_c^* for uniform QAM, and (b) optimal code rate R_c^* (solid lines) and optimal shaping rate R_s^* normalized by m (dashed lines) for PS QAM.

rates to the form

$$R_c = \frac{z k_b}{z n_b} = \frac{k_c}{n_c}, \tag{1}$$

resulting in a coding overhead of $(n_b - k_b)/k_b$, with k_b and n_b being small positive integers. Hence, practically achievable code rates have a relatively coarse granularity and do not fall on a uniform grid; e.g., the 9 code rates of Fig. 3, $R_c = 1/2, 2/3, \ldots, 9/10$, have increments of 0.167, 0.083, ... , 0.011. Together with a set of uniform M^2-ary QAM constellations, this leads to IRs of[1]

$$IR = 2mR_c \tag{2}$$

in bits/symbol (per two dimensions: in-phase I and quadrature Q), where $m = \log_2 M$. Therefore, with uniform QAM and multi-rate FEC, one can only obtain coarse and irregular IR increments, as shown in Fig. 3.

The AIR is determined through the *mutual information (MI)* or *generalized MI (GMI)*, which will be discussed in Section III in more detail. We denote the AIR under a given transponder constraint by IR^*. Once IR^* is obtained for a given QAM order and SNR, the required code rate R_c^* is found as, cf. (2),

$$R_c^* = IR^*/(2m), \tag{3}$$

which is depicted in Fig. 4(a) for various uniform square QAM formats as a function of the SNR. Note that R_c^* denotes the theoretically largest code rate that leads to error-free decoding; any actually used FEC code must have a rate smaller than R_c^*. The available code rates may potentially be far from the optimum rate R_c^*, which consequently leads to the step function behavior of Fig. 3. In order to obtain finer granularity than given by the "mother codes", codes can be *shortened* or *punctured* [48]–[52]. By shortening or puncturing s code symbols in each codeword, with $s \ll n_c$, code rates of $(k_c - s)/n_c < R_c$ or $k_c/(n_c - s) > R_c$ can be derived with a step size $\Delta_{R_c} \approx 1/n_c$, letting the resulting code rate more closely approach R_c^*. Since the code length n_c is generally beyond tens of thousands in

[1]Note that the IR is a property of the transponder parameters alone, while the AIR is a property of the channel, possibly constrained by assumptions on the transponder as well (cf. Table I in Section III).

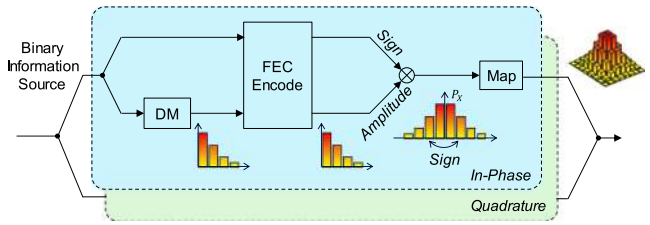

Fig. 5. The PAS architecture [33].

optical fiber communications, the rate discrepancy $\lesssim 1/(2n_c)$ between the optimal R_c^* and the realized R_c could then be made negligible and one could thereby make the steps finer and more closely approach the modulation-constrained AIR of Fig. 3. However, shortening or puncturing induces two problems in practice: *(i)* shortened or punctured codes generally have a wider gap to the AIR than the mother code [48]–[50], which can often be significant in practice [51], [52], because the optimal degree distribution for the rate of children codes may not necessarily be derived by shortening or puncturing the mother codes, and *(ii)* their error floor may be raised compared to the mother codes due to the change of their cycle properties, whose adverse effect must be minimized by a laborious optimization process [53]. The impact of suboptimum codes on system performance will be discussed in detail in Section IV.

2) PCS With Variable-Rate and Fixed-Rate FEC: As an alternative to uniform square QAM with variable-rate FEC, PCS can be used for rate adaptation in conjunction with variable-rate or even with fixed-rate FEC. As shown in Fig. 5, the PAS architecture [33] achieves PCS by independently shaping each signal dimension on an M-ary pulse amplitude modulation (PAM) template to construct a probabilistically-shaped (PS) M^2-QAM constellation. This is possible since the in-phase and quadrature dimensions of a modulated signal are orthogonal.

In what follows, we use the convention that a scalar random variable is denoted by a capital letter (e.g., X), a realization of a scalar random variable by a lowercase letter (e.g., x), and an alphabet (i.e., a set of allowed symbols) by a script letter (e.g., $\mathcal{X}$, with elements x_i). A vector of random variables is denoted by a boldface capital letter (e.g., $\boldsymbol{X}$), and a realization of a vector random variable by a boldface lowercase letter (e.g., $\boldsymbol{x}$).

Given the M-PAM symbol set $\mathcal{X} = \pm 1, \pm 3, \ldots, \pm(M-1)$, the probability of a constellation point $x \in \mathcal{X}$ is commonly generated according to the *Maxwell-Boltzmann (MB)* distribution

$$P_X(x) = \frac{e^{-\lambda x^2}}{\sum_{x' \in \mathcal{X}} e^{-\lambda x'^2}} \tag{4}$$

with $\lambda \geq 0$, which is the *maximum-entropy* distribution for $\mathcal{X}$ under an average-power constraint. The rate parameter λ controls the *entropy rate*[2] $2\mathbb{H}(X)$ of the PS QAM signal in bits/symbol, where $\mathbb{H}(X) = -\sum_{x \in \mathcal{X}} P_X(x) \log_2 P_X(x)$ denotes the binary entropy. When $\lambda = 0$, the MB distribution degenerates to a uniform distribution with $\mathbb{H}(X) = m$ bits/symbol per dimension. As λ increases, the MB distribution contains fractional numbers of $1 \leq \mathbb{H}(X) < m$ bits/symbol per dimension, hence realizing rate adaptation with a reduced average symbol energy. The functional block that performs rate-adaptive shaping in the PAS architecture is the *distribution matcher (DM)*, which transforms uniformly distributed input information bits to MB-distributed PAM output symbols, cf. Fig. 5. The DM generates only the positive amplitudes of the M -PAM symbols (a "half-PAM" constellation). A binary *systematic* FEC encoder generates parity bits that are equally distributed in $\{-1, +1\}$. Since the FEC code is systematic, it does not affect the information bits, so the positive-amplitude DM output remains unchanged by FEC encoding. A symmetric M -PAM distribution is then created by multiplying each of the half-PAM symbols with a parity bit acting as a sign bit. In some cases, the sign bit stream also includes some information bits in addition to parity bits, see [33], [54] for details.

In the PAS architecture with code rate R_c and entropy rate $2\mathbb{H}(X)$, the IR can be calculated as [33], [54]

$$IR = 2\left(\mathbb{H}(X) - m(1 - R_c)\right), \tag{5}$$

in bits/symbol per two dimensions. The term $2\mathbb{H}(P_X)$ on the right-hand side of (5) is the largest number of information bits that can be contained within a complex symbol (i.e., per two dimensions) with the distribution P_X, which is controlled by the rate parameter λ for an MB distribution, and the term $2m(1 - R_c)$ quantifies the FEC overhead in bits/symbol per two dimensions. Assuming bit-metric decoding (BMD, cf. Section III-B), IR^*, i.e., the largest AIR for a given SNR and QAM template, can be obtained by maximizing the GMI over all possible MB distributions P_X. The result then also represents the capacity of PAS in the auxiliary AWGN channel. The maximization can be done numerically by an exhaustive search or by the bisection method, since the MB distribution has only one free parameter λ. Rigorously speaking, IR^* obtained this way does not represent the *un*constrained AWGN channel capacity since *(i)* the finite number of constellation points in the underlying QAM template imposes a weak constraint on the modulation and *(ii)* the decoding is BMD. However, the gap between IR^* and the capacity of the auxiliary AWGN channel is negligible [55].

From (5), the required code rate R_c to achieve an IR with a channel input distribution P_X can be calculated as

$$R_c = 1 - \frac{\mathbb{H}(X) - IR/2}{m}. \tag{6}$$

If the DM produces a length-n_s amplitude block from a length-$(k_s - n_s)$ input bit block, with $k_s > n_s$, the sign path in the PAS architecture transports n_s sign bits per block, regardless of whether they are information bits or parity bits from a shaping point of view, hence the PAS architecture implements a *shaping rate* of

$$R_s = \frac{k_s}{n_s} \tag{7}$$

in bits/symbol per dimension [54]. While a class of FEC mother codes has a relatively low degree of freedom to choose k_c and n_c without shortening or puncturing, limiting the achievable rate adaptability as discussed above, there exists a DM algorithm that

[2]A stationary memoryless information source produces an entropy $\mathbb{H}(X_1, \ldots, X_n)$ that grows linearly with time n at a rate $\mathbb{H}(X)$, hence the name "entropy rate."

can finely adjust the number of input bits $k_s - n_s$ to be mapped into a length-n_s block of output symbols, hence achieves granularity of the shaping rate $\Delta_{R_s} = 1/n_s$. Denoting by X^* the M-PAM symbols that maximize the AIR through the MB distribution P_{X^*}, the small shaping granularity lets the realized R_s closely approach the optimal entropy rate $R_s^* \approx \mathbb{H}(X^*)$, by choosing a large block length n_s. Figure 4(b) shows the optimal shaping rate R_s^* (dashed lines) that produces the largest AIR in the auxiliary AWGN channel and the corresponding optimal code rate R_c^* obtained using (6) with $R_s^* = \mathbb{H}(X^*)$. As shown in the figure, when PCS shares the role of rate adaptation with FEC by adjusting both R_s and R_c, the optimal code rate *(i)* is much higher than when FEC alone performs rate adaptation (Fig. 4(a)), and *(ii)* occupies a much narrower range [55]; in the case of Fig. 4, we have $0.74 < R_c^* \leq 1$ for PCS, instead of $0.18 < R_c^* \leq 1$ for uniform QAM.

The narrow range of optimum FEC rates for PCS suggests the potential use of a *single* (or a small number of) fixed-rate FEC code(s), whereby rate adaptation is performed (almost) exclusively by PCS. This then gives a *code rate-constrained* AIR (with a weak modulation constraint given by the underlying QAM template). Remarkably, it was shown in [55] that the performance loss due to fixed-rate FEC with $R_c = 0.8$ does not exceed 0.07 bits/symbol of IR per two dimensions or 0.3 dB of SNR in the AWGN channel, valid for all square M^2-QAM templates with $M^2 \leq 1024$. This assumes ideal PCS with a DM that maps $k_s - n_s$ information bits into n_s PAM symbols such that the realized shaping rate $R_s = k_s/n_s$ is exactly equal to $\mathbb{H}(X^*)$. Such an ideal DM can be implemented, e.g., by constant composition distribution matching (CCDM) [56], which is asymptotically optimal in block length n_s. CCDM achieves close to optimal performance already with a relatively small $n_s \leq 10^4$, its hardware architecture is universal for all shaping rates $R_s \leq 2m$, and at least in principle it is implementable in today's hardware. Other DM techniques that are lower-complexity than CCDM at small performance loss are discussed in [57]–[63]. In contrast to shaping, it is extremely difficult for FEC to narrow down the last few tenths of a decibel of coding gap; for example, a rate-1/2 irregular and unstructured LDPC code with block length $n_c = 10^7$ and a maximum variable degree of 200 may approach the (modulation-constrained) AIR to within 0.04 dB at $BER = 10^{-6}$ using belief-propagation decoding with up to 2000 decoding iterations [64].

3) Time-Division Hybrid Modulation (TDHM): TDHM time-interleaves symbols picked from different uniform square QAM constellations in a deterministic manner to achieve fine granularity of the IR [65], [66]. For example, using M_1^2-QAM for a fraction $0 \leq \alpha \leq 1$ of the time, and M_2^2-QAM for a fraction $1 - \alpha$ of the time, TDHM can realize an arbitrary shaping rate of $R_s = \alpha m_1 + (1 - \alpha)m_2$ bits/symbol per dimension, where $m_1 = \log_2 M_1$ and $m_2 = \log_2 M_2$. When averaged over time, TDHM creates the illusion of an MB-like symbol distribution, cf. Fig. 6. However, TDHM is fundamentally different from *probabilistic* constellation shaping in that a receiver can separate the constituent constellations *deterministically* using the *a priori* knowledge of their temporal locations. (The same is true for any other hybrid modulation scheme that uses multiple orthogonal signal dimensions to carry different uniform QAM constellations in a deterministic manner, such as frequency-division hybrid modulation (FDHM) or digital subcarrier multiplexing [67], [68]). Consequently, while the *rate granularity* of TDHM can be as fine as that of PCS, the *performance* of TDHM does not reach that of PCS, as we shall see in the following section.

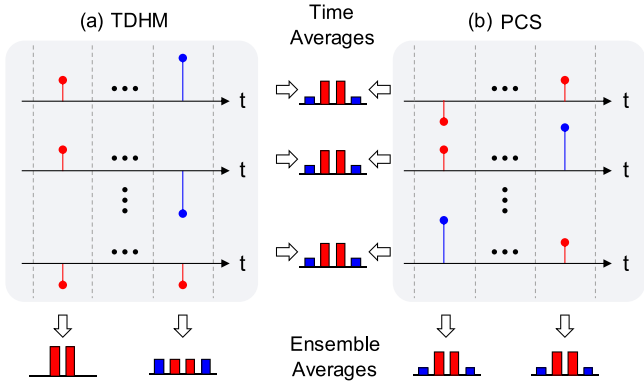

Fig. 6. Time and ensemble averages of symbols created by (a) TDHM and (b) PCS.

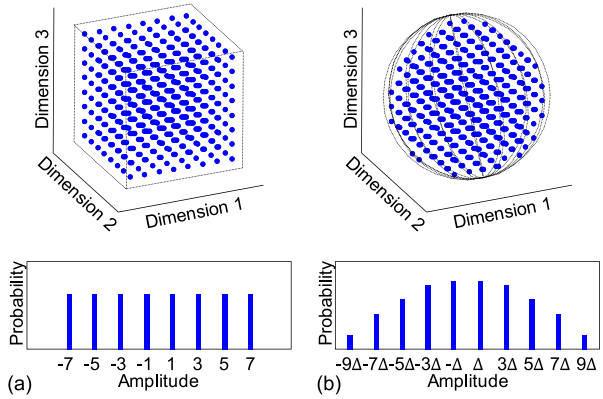

Fig. 7. Three-dimensional square lattice constellation points contained in (a) a cube, and (b) a ball, and their marginal probability distributions as projected onto each coordinate axis. Figure after [69].

C. Energy Efficiency

In this section, we illustrate various modulation schemes from the perspective of a multi-dimensional signal space, which gives valuable insights into why PCS is needed to closely approach the AWGN capacity. A set of 'dimensions' in signal space corresponds to the collection of any physically orthogonal entities, which may be most intuitively viewed as the real-valued (single-quadrature, PAM) amplitudes of consecutive symbols, which are orthogonal in time. Hence, 4 dimensions may be built by 4 successive PAM symbols. Alternatively, 4 dimensions may be built by 2 successive QAM symbols, or by a single polarization-division multiplexed (PDM) QAM symbol.

1) Uniform QAM: As shown in Fig. 7(a), assume an n_s-dimensional (hyper-) cube centered at the origin, each side being parallel with each of the n_s coordinate axes. If the cube is uniformly filled with points on a square lattice grid, the projection of any random selection of points onto any Cartesian

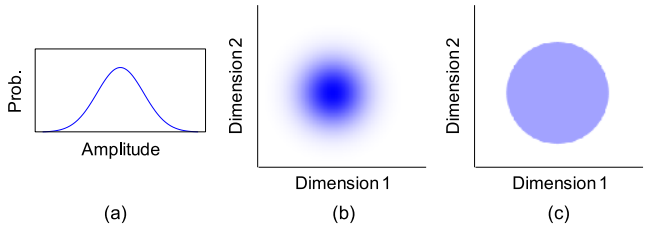

Fig. 8. (a) Gaussian distribution of a signal, (b) the two-dimensional 'fuzzy' ball with a non-uniform density created by their 2-fold Cartesian product, and (c) the two-dimensional uniform ball with the same entropy as that of (b).

coordinate axis yields a uniform distribution of points (i.e., a PAM constellation), regardless of the cardinality n_s. Projections on different axes are independent and identically distributed (IID). Conversely, the n_s -fold Cartesian product of zero-mean uniform IID distributions confined on a finite support constructs an n_s-dimensional uniform cube.

2) Probabilistic Constellation Shaping (PCS): Instead of the cube, now assume an n_s-dimensional (hyper-) ball centered at the origin, again with a uniform density of points within (cf. Fig. 7(b)). The projection onto any one of the Cartesian coordinate axes yields a *non-uniform* probability density. Since the energy of a signal point is quadratic in distance from the origin, a ball centered at the origin, which by definition is enclosed by a constant-radius surface, is the most energy efficient shape to contain a given number of points in multi-dimensional space. When $n_s = 3$, the points within the ball have ∼0.27 dB less average energy than those in the cube, assuming the same number of points (i.e., 512) and the same minimum distance (i.e., 2) between them. This relatively small energy saving is due to the small choice of n_s and the small number of points in this example, and increases with n_s.

The energy savings can be translated into a better noise resiliency in a communications context as follows: If the minimum distance of the ball is increased to ∼2.06 (i.e., $\Delta \approx 1.03$ in Fig. 7(b)) such that the average energy becomes the same for the ball and the cube, i.e., when we compare signals of equal energy or signals of equal SNR, the points in the ball have now an increased minimum distance, hence are more immune to noise. This suggests that transmitting discrete information symbols in n_s dimensions (e.g., by transmitting successively in n_s time slots), the tightly enclosing shape of the symbols should be an n_s-dimensional ball instead of an n_s-dimensional cube.

As $n_s \to \infty$, and as the number of points on each axis $M \to \infty$, the probability density of the points projected onto each coordinate axis converges to a Gaussian distribution. Conversely, if we generate an IID zero-mean Gaussian signal in every Cartesian coordinate axis, the composite signal in n-dimensional space forms a uniformly dense ball as $n_s \to \infty$. Note that this statement only applies for $n_s \to \infty$, as composite points generated from a finite number of IID Gaussian amplitude distributions will generally result in a 'fuzzy' ball with a non-uniform density, not a true ball with a uniform density, as shown in Fig. 8. The energy savings (i.e., the shaping gain) of a ball relative to a cube for the same volume approaches $\pi e/6 \approx 1.53$ dB [70], Ch. 14] in the limit of $n_s \to \infty$. While the above considerations apply to the constellation entropy (a property of the transmitter), it can be shown that Gaussian signals also result in maximum mutual information between the transmitted and the received signals under a transmission energy constraint in the presence of AWGN [70], Ch. 3], [71], Chs. 8, 9].

True Gaussian signaling requires continuous symbols whose support is not confined to within a finite range of amplitudes. This leads to high required digital-to-analog and analog-to-digital converter resolutions and to large peak-to-average power ratios, which are both problematic engineering aspects in practice. If the symbols are discrete and confined to a finite range on each coordinate axis, it can be shown that the distribution that maximizes the entropy is an MB distribution [5], which is a Gaussian distribution sampled at discrete amplitudes across a finite amplitude range, cf. (4). Here, it should be noted that a continuous Gaussian distribution maximizes both the entropy and the AIR under a transmission energy constraint, but the MB distribution is proven to maximize only the entropy, not the AIR, the latter being maximized using the Blahut-Arimoto algorithm [72], [73]. Nevertheless, the AIR obtained by the MB distribution is very close to the AWGN channel capacity [33].

Creating the shaped distribution in each dimension is the task of the DM. For example, the CCDM algorithm creates a target distribution by fixing the number of occurrences of M-PAM symbols in each length-n_s block; i.e., symbol $x_i \in \mathcal{X}$, for $i = 1, \ldots, M$, appears exactly n_i times in each of the length-n_s CCDM blocks, where $n_s = \sum_{i=1}^{M} n_i$, thereby creating a probability mass function (PMF) $P_X = [\frac{n_1}{n_s}, \ldots, \frac{n_M}{n_s}]$ that approximates an MB distribution. Therefore, if we mark a constellation point in n_s-dimensional space, whose coordinates are specified by the n_s symbols of the CCDM block, its distance from the origin is a constant $\sqrt{\sum_{i=1}^{M} n_i |x_i|^2}$, hence it lies on an n_s-dimensionl spherical shell. Knowing that almost the entire volume of a ball is near the surface in high-dimensional space (known as the *sphere hardening* phenomenon [70]), CCDM casts symbols onto the surface of a ball as $n_s \to \infty$, which is a *necessary* condition to achieve the optimal energy efficiency. A *sufficient* condition for the optimal energy efficiency under the constraint on the finite support on each coordinate axis is that the DM maps each of the points in a k_s-dimensional uniform cube to a distinct point in an n_s-dimensional ball (truncated to within a finite support in each dimension), thereby fulfilling $R_s = k_s/n_s \to \mathbb{H}(X)$, where P_X is an MB distribution. This is fulfilled by CCDM, as the block length $n_s \to \infty$. However, if the block length n_s is small, R_s is smaller than $\mathbb{H}(X)$, and the volume inside the surface of the ball is not negligible, hence CCDM becomes sub-optimal. In this case, a direct mapping of uniformly distributed information bits to a completely filled n_s -dimensional ball-like constellation can outperform CCDM, as is done, e.g., by shell mapping [63], [74]–[76].

3) Time-Domain Hybrid Modulation (TDHM): When speaking of 'constellation shaping' it is important to distinguish between *ensemble*-averages and *time*-averages, as visualized in Fig. 6. The *time average* over all symbols in a data stream may yield the same symbol amplitude distribution for both TDHM and PCS, in fact, the overall amplitude distribution averaged over all symbols in a TDHM stream may even be MB, and this

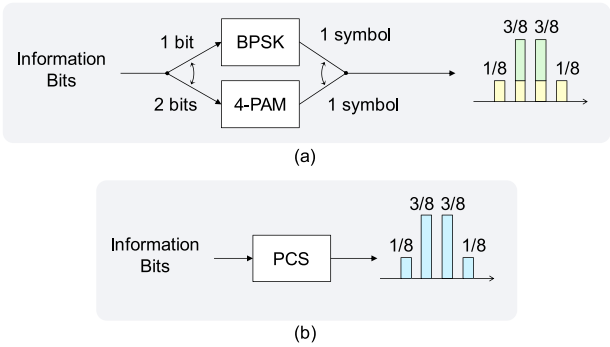

Fig. 9. Time-averaged distributions generated (a) by TDHM, and (b) by PCS.

may suggest that TDHM and PCS should perform the same in terms of their shaping characteristics. However, the *ensemble average*, i.e., the symbol amplitude distribution within a single time slot when averaged across all possible data streams, looks very different for the two shaping schemes, as shown in Fig. 6. In an ideal PCS implementation, ensemble average and time average result in the same distribution, letting the encoding process be stationary and ergodic, and justifying the AIR calculated based on the entropy as in (5) [77]. As an example, consider the TDHM shown in Fig. 9(a) that interleaves symbols drawn from a uniform binary phase-shift keying (BPSK) alphabet $\mathcal{X}_{\text{BPSK}} = [-1, +1]$ and symbols drawn from a 4-PAM alphabet $\mathcal{X}_{\text{4-PAM}} = [-3, -1, +1, +3]$ at a multiplexing ratio $\alpha = 0.5$ such that an MB distribution $P_X = [p_1, \ldots, p_4] = [\frac{1}{8}, \frac{3}{8}, \frac{3}{8}, \frac{1}{8}]$ is observed at the receiver when performing a time average. The shaping rate of this TDHM is $R_s = (1+2)/2 = 1.5$ bits/symbol per dimension, and the average symbol energy is $\sum_{m=1}^{4} p_m |x_m|^2 = 3$. Note that PCS can create the same time-averaged distribution (hence the same average symbol energy of 3), as shown in Fig. 9(b), but it can do so at a larger shaping rate of $R_s = \mathbb{H}(X) \approx 1.8$ bits/symbol per dimension! This shows that achieving a time-averaged MB distribution is only a necessary condition for optimal energy efficiency.

By using different PAM orders in different time slots, TDHM does not construct a ball but rather constructs a (hyper-) rectangle. As it is the cube (with equal side lengths) that is the most energy-efficient shape among all possible rectangles for the same volume, TDHM performs worse than uniform square-QAM; and as the ball is more energy efficient than the cube, PCS performs best. Figure 10 depicts a two-dimensional example, representing square-QAM and TDHM in 2 dimensions. The points in the rectangle have ∼3.3 dB larger average energy than the points in the cube, with the same number of points (i.e., 64) and the same minimum distance (i.e., 2). The same is evident from Figure 11, which shows that TDHM (lower solid line) can cause a loss of ∼2 dB in SNR [69], or 25% loss in AIR [78], relative to optimal PCS (upper solid line) in the AWGN channel, when all bit levels are encoded jointly by a single FEC code of rate 0.8. If used with a fixed rate-0.8 FEC code, TDHM performs worse than uniform square QAMs with rate-adaptable FEC (cf. dashed lines in Fig. 11). A comparison of rate adaptability and performance of the various coded modulation schemes discussed so far are sketched in Fig. 12.

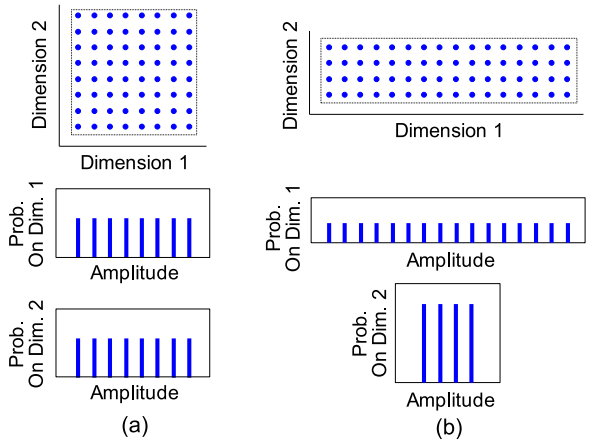

Fig. 10. Two-dimensional square lattice constellation points contained in (a) a cube, and (b) a rectangle, and their marginal probability distributions in each coordinate axis.

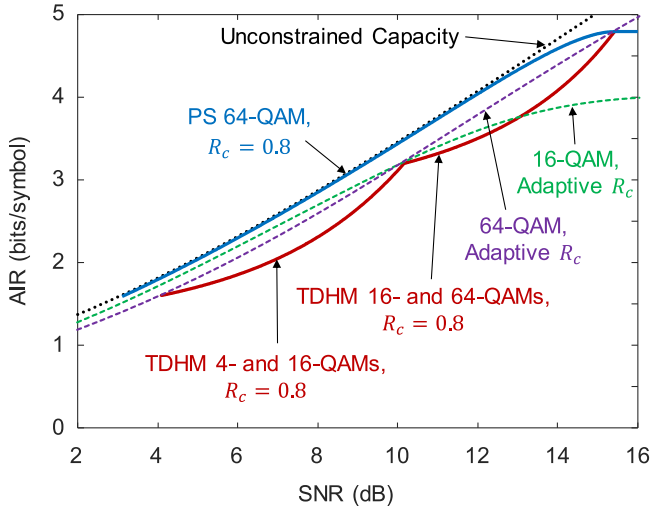

Fig. 11. AIR of various modulation schemes under bit metric decoding in the AWGN channel.

TABLE I
PERFORMANCE METRICS FOR PCS

	Optimal SMD, Optimal PCS	Optimal BMD, Optimal PCS	Sub-Optimal BMD, Sub-Optimal PCS
Channel Metrics	$MI(X^*;Y)$ $NMI(X^*;Y)$	$GMI(X^*;Y)$ $NGMI(X^*;Y)$	$GMI(X^\dagger;Y)$ $NGMI(X^\dagger;Y)$
Transceiver Metrics	$R_s^* = \mathbb{H}(X^*)$ $R_c^* = NMI(X^*;Y)$	$R_s^* = \mathbb{H}(X^*)$ $R_c^* = NGMI(X^*;Y)$	$R_s = (1-\delta_s)\mathbb{H}(X^\dagger)$ $R_c = \big(NGMI(X^\dagger;Y) - (1+\delta_c)\big) \times (1-\delta_s) + 1$

III. PERFORMANCE METRICS FOR PCS

To quantify system performance of PCS in conjunction with SD FEC, several approaches with and without an explicit focus on their operational meaning have been taken [79]–[85]. Relevant performance metrics are summarized in Table I. The system model used to obtain these metrics is depicted in Fig. 13(a).

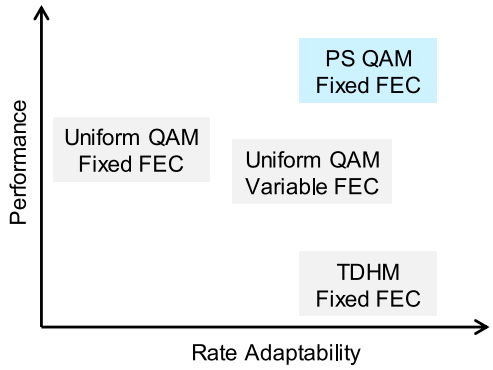

Fig. 12. Rate adaptability and performance of various schemes.

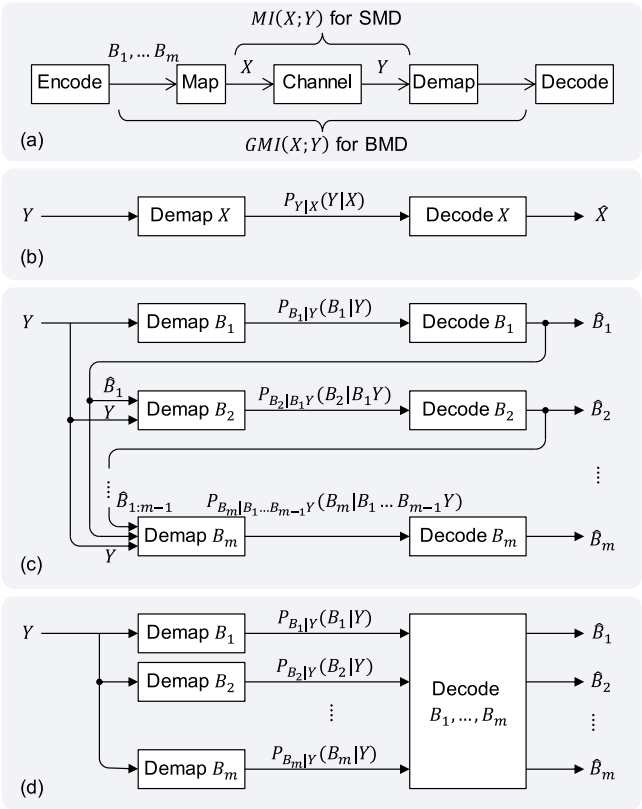

Fig. 13. (a) System model, and architecture of decoders for (b) SMD, (c) multi-level coding and multi-stage decoding (discussed in Appendix), and (d) BMD.

We first consider SMD with non-binary FEC codes that have the same number of symbols in the code alphabet as that of the modulation alphabet, i.e., M-ary FEC codes for an M-ary constellation. (In principle, the code alphabet need not have the same cardinality as the modulation alphabet, but this restriction makes it simple to develop equations and achieves capacity in a memoryless channel.) As briefly discussed in Section II-B.1, a relevant performance metric for SMD is the MI that quantifies an IR that is *achievable* (hence an AIR) using infinite code length and unlimited decoder complexity. The channel capacity, known as the Shannon limit (SL), is obtained by maximizing the MI over all possible modulation formats (including continuous-amplitude formats with infinitely many "constellation points").

For the more practical class of BMD systems, a bit-to-symbol mapper transforms an m-bit sequence $[B_1, \ldots, B_m]$ to an M-ary modulation symbol X, cf. Fig. 13(a), where $m = \log_2 M$. If the bit sequences are encoded by binary FEC codes and are decoded using BMD, and if we still allow infinite code length and unlimited decoder complexity, the GMI represents an AIR for BMD, in the same way as the MI represents an AIR for SMD. Maximizing the GMI over all possible input symbol distributions for a square QAM template yields an AIR that is constrained in terms of the code alphabet size, the specific modulation template, and the fact that we are using BMD. In this section, without imposing any complexity constraints on FEC and PCS, we review the MI, GMI, and other related metrics in the context of the underlying transponder architecture. A more realistic scenario will be discussed in Section IV, where practical (non-ideal, pragmatic) FEC and complexity-constrained PCS are assumed.

A. Mutual Information

Assume that we use a length-n_c M-ary SD FEC code with code rate $R_c = k_c/n_c$ together with an M-ary constellation, and the (auxiliary) channel is memoryless AWGN. In this system, based on perfect knowledge of the transmitted symbols X, a measurable statistic of the channel is $P_{Y|X}(Y|X)$, i.e., the probability of the observed physical entity Y given the transmitted physical entity X, cf. Fig. 13(b), which is often called the *channel transition probability*. An SD demapper produces the conditional probability $P_{Y|S}(y_i|s)$ of the i-th received symbol y_i, for $i = 1, \ldots, n_c$, for every symbol s in the code alphabet. In our system where the FEC code has the same alphabet size as the constellation, this is equivalent to the conditional probability $P_{Y|X}(y_i|x)$given a transmitted modulation symbol $x \in \mathcal{X}$, which is directly fed to the subsequent SMD as an SD decoding metric. An optimal SMD finds a *legitimate codeword* $\boldsymbol{x} = [x_1, \ldots, x_{n_c}]$ that is the most likely to be transmitted among all M^{k_c} possible codewords, given the noisy observation $\boldsymbol{y} = [y_1, \ldots, y_{n_c}]$, by maximizing the product of the channel transition probabilities over all symbols in $\boldsymbol{y}$, $P_{\boldsymbol{Y}|\boldsymbol{X}}(\boldsymbol{y}|\boldsymbol{x}) = \prod_{i=1}^{n_c} P_{Y|X}(y_i|x_i)$ [71], Ch. 7.7]. It should be noted that there are only M^{k_c} codewords that are legitimate for the underlying code, while M^{n_c} *uncoded* sequences can exist for an M-ary alphabet. Therefore, only one out of $M^{n_c}/M^{k_c} = M^{n_c(1-R_c)}$ possible words is a legitimate codeword, which allows a decoder to select the nearest codeword from a noisy non-codeword word. (This illustrates the fundamental operation of FEC.) An AIR of the ideal and optimal SMD is the MI, defined as

$$\begin{aligned}\mathbb{I}(X;Y) &\triangleq \mathbb{E}_{X,Y}\left[\log_2 \frac{P_{Y|X}(Y|X)}{P_Y(Y)}\right] \\ &= \mathbb{E}_{X,Y}\left[\log_2 \frac{P_{Y|X}(Y|X)}{\sum_{x' \in \mathcal{X}} P_X(x') P_{Y|X}(Y|x')}\right] \quad (8)\end{aligned}$$

in bits/symbol per dimension, where X is a random variable for the one-dimensional transmitted signal, Y is a random variable

for the corresponding received signal in the AWGN channel with a known noise variance, and $\mathbb{E}_{X,Y}(\cdot)$ denotes the expectation taken over X and Y. Here, by "ideal" SMD, we mean that a code is of infinite length ($n_c \to \infty$), and by "optimal" SMD, we mean that *(i)* the code rate R_c is chosen to match the channel condition, and *(ii)* no other codeword has a higher likelihood than the codeword chosen by SMD, since the decoder is (unrealistically) capable of sorting all M^{k_c} codewords in a descending order of their probabilities $P_{\boldsymbol{Y}|\boldsymbol{X}}(\boldsymbol{y}|\boldsymbol{x})$. The supremum of (8) over all possible (continuous- and discrete-amplitude) input distributions P_X is the channel capacity, which on an (auxiliary) AWGN channel can be achieved by Gaussian signaling, as discussed in Section II.

Although it is in principle possible to use non-binary codes and SMD in the PAS architecture, PCS in optical systems is commonly implemented using binary codes and BMD for complexity reasons, hence the MI does not generally represent the most relevant performance metric.

B. Generalized Mutual Information

Let us next consider BMD in Fig. 13(a), where a bit-to-symbol mapper transforms a vector $\boldsymbol{B} \triangleq [B_1, \ldots, B_m]$ to a symbol X of an M-PAM constellation. It should be first noted that B_j for $j = 1, \ldots, m$ are logical entities that are not directly cast into the channel, but only through their physical representation X, e.g., a voltage or an optical field amplitude. On the other hand, in the context of BMD, the decoder estimates *bits* and not *symbols*. Therefore, the decoder operates on $P_{Y|B_j}(Y|B_j)$ instead of $P_{Y|X}(Y|X)$, calculated as

$$P_{Y|B_j}(Y|B_j) = \frac{P_{B_j,Y}(B_j,Y)}{P_{B_j}(B_j)} = \frac{\sum_{x' \in \mathcal{X}_{b_j(x)}^{(j)}} P_{Y|X}(Y|x') P_X(x')}{P_{B_j}(B_j)},$$

where $b_j(x)$ is the j-th bit of symbol x, and $\mathcal{X}_b^{(j)} \triangleq \{x \in \mathcal{X} : b_j(x) = b\}$ denotes the set of constellation points x whose j-th bit representation is $b \in \{0, 1\}$. For example, if we use binary reflected Gray coding (BRGC) {101, 100, 110, 111, 011, 010, 000, 001} to represent the 8-PAM symbol alphabet $\mathcal{X} = \{-7, -5, \ldots, +7\}$, the symbol sets corresponding to a '0' and '1' at the second bit position are $\mathcal{X}_0^{(2)} = \{-7, -5, +5, +7\}$ and $\mathcal{X}_1^{(2)} = \{-3, -1, +1, +3\}$, respectively. The conditional probability of observation y given transmitted bit $B_2 = 0$ is then calculated through $P_{Y|X}(Y|X)$ as $P_{Y|B_2}(y|0) = \sum_{x' \in \mathcal{X}_0^{(2)}} P_{Y|X}(y|x') P_X(x') / P_{B_2}(0)$. In BMD, we often use the conditional *likelihood* $P_{B_j|Y}(B_j|Y)$ instead of the conditional *probability* $P_{Y|B_j}(Y|B_j)$, which can be obtained by Bayes' rule as

$$P_{B_j|Y}(B_j|Y) = P_{Y|B_j}(Y|B_j) \frac{P_{B_j}(B_j)}{P_Y(Y)} = \frac{\sum_{x' \in \mathcal{X}_{b_j(x)}^{(j)}} P_{Y|X}(Y|x') P_X(x')}{P_Y(Y)}, \quad (9)$$

which represents the SD decoding metric of BMD. An SD demapper for BMD produces the conditional likelihood $P_{B_j|Y}(b_{i,j}|y_i)$ for the j-th bit $b_{i,j}$ of the i-th transmitted symbol x_i, for $i = 1, \ldots, n_c$, which is then input to the subsequent binary SD decoder, cf. Fig. 13(d). Here, we omit the time index i from $B_{i,j}$ and Y_i since the PCS encoding is a stationary process and the channel is assumed to be stationary as well. For a length-n_c binary code, optimal BMD finds a legitimate codeword $\boldsymbol{b} = [b_{1,1}, \ldots, b_{n_c/m,\,m}]$ that is the most likely to be transmitted among all 2^{k_c} possible codewords by maximizing $P_{\boldsymbol{B}|\boldsymbol{Y}}(\boldsymbol{b}|\boldsymbol{y}) = \prod_{i=1}^{n_c/m} \prod_{j=1}^{m} P_{B_{i,j}|Y}(b_{i,j}|y_j)$, given the noisy observation $\boldsymbol{y} = [y_1, \ldots, y_{n_c/m}]$. Multiplications in $P_{\boldsymbol{B}|\boldsymbol{Y}}(\boldsymbol{b}|\boldsymbol{y})$ are often removed by taking the logarithm without affecting the decoding performance. In addition, instead of producing two metrics $P_{B_j|Y}(0|y_i)$ and $P_{B_j|Y}(1|y_i)$ for each received symbol y_i, the SD BMD demapper can produce only one log-likelihood ratio (LLR) metric

$$\log \frac{P_{B_j|Y}(0|y_i)}{P_{B_j|Y}(1|y_i)}, \quad (10)$$

which will be discussed in Section IV in more detail. Note that the BMD demapper produces only $\log_2 M$ LLRs per received symbol, whereas an SMD demapper produces $|\mathcal{X}| = M$ LLRs per received symbol, in the form of $\log P_{X|Y}(x_1|y_i)/P_{X|Y}(x|y_i)$ for all $x \in \mathcal{X}$, where x_1 denotes the first letter in $\mathcal{X}$. Using the conditional likelihood $P_{B_j|Y}(B_j|Y)$ in (9), the channel transition probability can be approximated as (see Appendix for derivation details and for a clarification of the operational meaning of the obtained results)

$$Q_{Y|X}(Y|X) \triangleq \left[\prod_{j=1}^{m} P_{B_j|Y}(B_j|Y)\right] \frac{P_Y(Y)}{P_X(X)} \approx P_{Y|X}(Y|X). \quad (11)$$

This is called the *mismatched* decoding metric [86], [87], since $Q_{\boldsymbol{Y}|\boldsymbol{X}}(\boldsymbol{y}|\boldsymbol{x}) = \prod_{i=1}^{n_c/m} Q_{Y|X}(y_i|x_i)$ is not a monotonic function of $P_{\boldsymbol{Y}|\boldsymbol{X}}(\boldsymbol{y}|\boldsymbol{x})$, causing loss of decoding performance; in other words, the codeword that maximizes $Q_{\boldsymbol{Y}|\boldsymbol{X}}(\boldsymbol{y}|\boldsymbol{x})$ does not necessarily maximize $P_{\boldsymbol{Y}|\boldsymbol{X}}(\boldsymbol{y}|\boldsymbol{x})$.

Eventually, in analogy to the MI obtained from the exact decoding metric $P_{Y|X}(Y|X)$ as in (8), we obtain the GMI using the approximate decoding metric $Q_{Y|X}(Y|X)$ as

$$GMI(X;Y) \triangleq \mathbb{E}_{X,Y}\left[\log_2 \frac{Q_{Y|X}(Y|X)}{\sum_{x' \in \mathcal{X}} P_X(x') Q_{Y|X}(Y|x')}\right] \quad (12)$$

in bits/symbol per dimension. After some mathematical manipulation (see Appendix), we can obtain a compact notation of (12) as

$$GMI(X;Y) = H(X) - \sum_{j=1}^{m} \mathbb{H}(B_j|Y). \quad (13)$$

In case of uniform P_X and independent bit levels, (13) degenerates to

$$GMI(X;Y) = \sum_{j=1}^{m} \mathbb{I}(B_j;Y),$$

which represents an AIR for bit-interleaved coded modulation (BICM) [87]. Importantly, the GMI in (13) has the same form as the "BMD rate" that was first defined in [33], and was proven

to be *achievable* [82], i.e., there exists a coding scheme such that the post-FEC BER can be made arbitrarily small, as the code length $n_c \to \infty$. The supremum of GMI over all possible P_X is the capacity of PCS under the constraints of a square QAM template and parallel BMD, which can be approximately achieved by an MB distribution.

C. Normalized Generalized Mutual Information

The GMI quantifies the number of information bits *per transmitted symbol* that can be reliably transmitted through a given channel. After proper normalization of the GMI, we can derive a channel metric that quantifies the number of information bits *per transmitted bit*, which is called the *normalized GMI (NGMI)* [79]–[81]. Since the GMI is an AIR of the PAS architecture as per our above discussion, we can replace the IR of (5) with the GMI to obtain the unit-less metric

$$NGMI\left(X;Y\right) = 1 - \tfrac{\mathbb{H}(X) - GMI(X;Y)}{m}. \tag{14}$$

It immediately follows from (13) and (14) that

$$NGMI\left(X;Y\right) = 1 - \tfrac{1}{m}\textstyle\sum_{j=1}^{m} \mathbb{H}\left(B_j\,|Y\right). \tag{15}$$

Note that the asymmetric information (ASI) introduced in [85] from a different perspective has the same form as the NGMI.

Suppose that we have obtained the maximum $GMI(X;Y)$ over all possible distributions of X, and denote by X^* the channel input that maximizes the GMI, i.e., $X^* = \mathrm{argmax}_X\, GMI(X;Y)$. It should be noted that $GMI(X^*;Y)$ and $NGMI(X^*;Y)$ are not associated with potential imperfections of the underlying transceiver technology but represent *channel metrics* of the auxiliary AWGN channel, whereas R_c^* in (1) and R_s^* in (7) are the *transceiver metrics* that need to be used to *achieve* $GMI(X^*;Y)$, cf. Table I. In other words, the channel's transmission capabilities as given by the channel metric $GMI(X^*;Y)$ are fully exhausted when we use ideal binary FEC with the optimal code rate $R_c^* = NGMI(X^*;Y)$ and ideal PCS with the optimal shaping rate $R_s^* = \mathbb{H}(X^*)$, as summarized in Table I.

IV. Impact of Sub-Optimal PCS and FEC

GMI and NGMI quantify theoretic channel metrics as well as the limit of transceiver technologies without imposing any constraints on implementation complexity. However, they are also very useful to evaluate and optimize systems with sub-optimal pragmatic PCS and FEC, if shaping and coding gaps are properly taken into account. In what follows, let $P_{X^\dagger}$ denote the distribution that maximizes the IR using a *sub-optimal* PCS and/or FEC scheme.

A. Sub-Optimal FEC, Optimal Shaping

Since sub-optimal FEC requires more redundancy (i.e., a lower code rate) than optimal FEC to achieve error-free decoding, the largest code rate for error-free decoding is

$$R_c^\dagger = NGMI\left(X^\dagger;Y\right) - \delta_c,$$

where $\delta_c \geq 0$ is the *coding gap*. The coding gap δ_c quantifies how much *fewer* information bits are conveyed per transmitted bit by sub-optimal coding compared to optimal coding. In [80], FEC decoding simulations are performed using spatially-coupled (SC) LDPC codes, showing that for each code rate $R_c^\dagger$ the coding gap δ_c is nearly constant across various distributions P_X and M^2-QAM constellation templates; the most widely applicable coding gap is conservatively chosen as that of the smallest constellation (i.e., 4-QAM) since it is the marginally greatest among those of all P_X and M^2-QAM. This implies that we can with high confidence declare error-free decoding if the channel metric $NGMI(X^\dagger;Y)$ is larger than the code rate $R_c^\dagger$ by δ_c, independent of modulation. Therefore, if only one FEC code of rate r_c with coding gap δ_c is available, the optimal shaping distribution can be obtained as

$$\begin{aligned} P_{X^\dagger} = &\operatorname*{argmax}_{P_X} GMI\left(X;Y\right) \\ &\text{subject to} \quad NGMI\left(X;Y\right) \geq r_c + \delta_c, \end{aligned} \tag{16}$$

where the last condition ensures error-free decoding. It has been shown in [88] that the loss of IR due to a constant coding gap δ_c is approximately proportional to m, which importantly implies that a small QAM template with moderate shaping performs better than a large QAM template with strong shaping.

B. Optimal FEC, Sub-Optimal Shaping

If the FEC is optimal but PCS is sub-optimal, we can calculate the IR loss $\Delta_s \geq 0$ that quantifies how many *fewer* information bits are transmitted per transmitted symbol per dimension by a sub-optimal shaping algorithm compared to optimal shaping. Formally, the IR loss due to a sub-optimal shaping algorithm is $\Delta_s \triangleq \mathbb{H}(X^\dagger) - R_s^\dagger$, where $X^\dagger$ is the output of the sub-optimal shaping algorithm whose probability approximately follows an MB distribution and $R_s^\dagger \leq \mathbb{H}(X^\dagger)$ is the realized shaping rate (7). If we define a shaping gap as the unit-less ratio of the IR loss relative to the entropy $\mathbb{H}(X^\dagger)$ for the same average symbol energy $\mathbb{H} * [|X^\dagger|^2\,]$, i.e.,

$$\delta_s \triangleq \frac{\Delta_s}{\mathbb{H}\left(X^\dagger\right)} = 1 - \frac{R_s^\dagger}{\mathbb{H}\left(X^\dagger\right)},$$

the IR obtained by sub-optimal shaping is a fraction $R_s^\dagger/\mathbb{H}(X^\dagger) = 1 - \delta_s \leq 1$ of the GMI. Also, by substituting $R_s^\dagger$ for $\mathbb{H}(X^\dagger)$ in (5), we have

$$\begin{aligned} IR &= R_s^\dagger - m\left(1 - R_c^\dagger\right) \\ &= \mathbb{H}\left(X^\dagger\right)(1-\delta_s) - m\left(1 - R_c^\dagger\right) \end{aligned}$$

in bits/symbol per dimension. It follows from $IR = GMI(X^\dagger;Y)(1-\delta_s)$ that the optimal code rate that achieves this IR is then given by

$$\begin{aligned} R_c^\dagger &= 1 - \frac{\mathbb{H}\left(X^\dagger\right) - GMI\left(X^\dagger;Y\right)}{m}(1-\delta_s) \\ &= NGMI\left(X^\dagger;Y\right)(1-\delta_s) + \delta_s. \end{aligned} \tag{17}$$

If only one FEC code of rate r_c with $\delta_c = 0$ is available, and if the shaping gap δ_s is known for every realized MB distribution P_X of the shaping algorithm, the optimal distribution for this

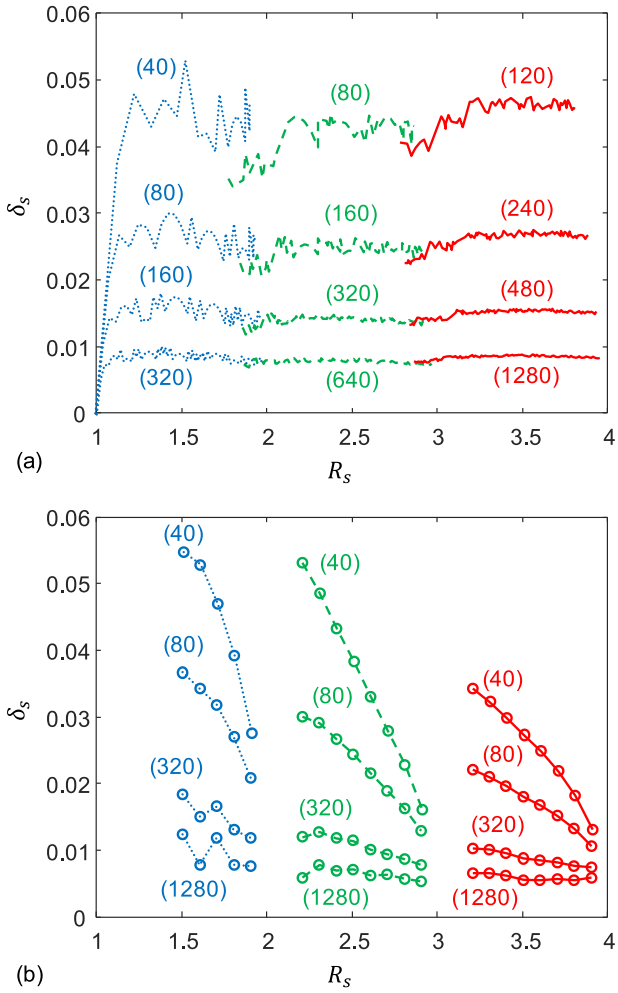

Fig. 14. Shaping gap δ_s of (a) CCDM and (b) MR-PCDM, with 4-PAM (dotted lines), 8-PAM (dashed lines), and 16-PAM (solid lines) constellations. The numbers in parentheses show the block length n_s.

sub-optimal shaping scheme can be obtained by

$$P_{X^\dagger} = \underset{P_X}{\operatorname{argmax}}\, GMI\left(X;Y\right)$$

$$\text{subject to} \quad NGMI\left(X;Y\right) \geq \frac{r_c - \delta_s}{1-\delta_s}. \tag{18}$$

In Fig. 14, the shaping gap is estimated for two sub-optimal finite-length DM algorithms: (a) CCDM [56], and (b) low-complexity multi-rate prefix-free code DM (MR-PCDM) [89]. For some cases in Fig. 14, the shaping gap is almost constant across the realized shaping rates R_s, e.g., when $n_s \geq 320$ with CCDM, or when $n_s \geq 1280$ with MR-PCDM for 8- and 16-PAMs. This constant shaping gap simplifies the maximization problem (18) and facilitates the analysis, as will be shown in the following section.

C. Sub-Optimal FEC and Sub-Optimal Shaping

Combining the above results, if FEC and PCS are *both* sub-optimal, after penalizing GMI by δ_c and δ_s, the IR can be calculated as

$$IR = \left(GMI\left(X^\dagger;Y\right) - m\delta_c\right)\left(1-\delta_s\right). \tag{19}$$

At the same time, from (5) we have

$$IR = H\left(X^\dagger\right)\left(1-\delta_s\right) - m\left(1-R_c^\dagger\right) \tag{20}$$

in bits/symbol per dimension. Therefore, the optimal code rate is given by relating (19) and (20) as

$$R_c^\dagger = \left(NGMI\left(X^\dagger;Y\right) - \left(1+\delta_c\right)\right)\left(1-\delta_s\right) + 1. \tag{21}$$

In case where a fixed rate-r_c code is used with a pre-determined coding gap δ_c, if we assume a nearly constant shaping gap of δ_s over all R_s, (20) shows that the practically achieved IR is increasing with the entropy rate $\mathbb{H}(X^\dagger)$. Therefore, the optimal distribution $P_{X^\dagger}$ for the sub-optimal PCS and FEC can be obtained by solving

$$P_{X^\dagger} = \underset{P_X}{\operatorname{argmax}}\, \mathbb{H}\left(X\right)$$

$$\text{subject to} \quad NGMI\left(X;Y\right) \geq \frac{r_c - \delta_s}{1-\delta_s} + \delta_c. \tag{22}$$

Figures 15 and 16 show the IRs obtained by solving the maximization problem (22), with coding gaps $\delta_c = 0, 0.05, 0.1$, and shaping gaps $\delta_s = 0, 0.025, 0.05$. Note that state-of-the-art soft-decision FEC codes have coding gaps of $\delta_c \leq 0.1$, and CCDM with a block length ≥ 480 produces shaping gaps of $\delta_s \lesssim 0.02$, as shown in Fig. 14(a). It can be seen from Figs. 15 and 16 that a reduction of the *coding gap* is crucial to more closely approach the channel capacity, but the effect of a *shaping gap* on the IR is relatively insignificant, except at high SNR where the IR is saturated. In practice, however, the IR at high SNR can be recovered if uniform QAM is used.

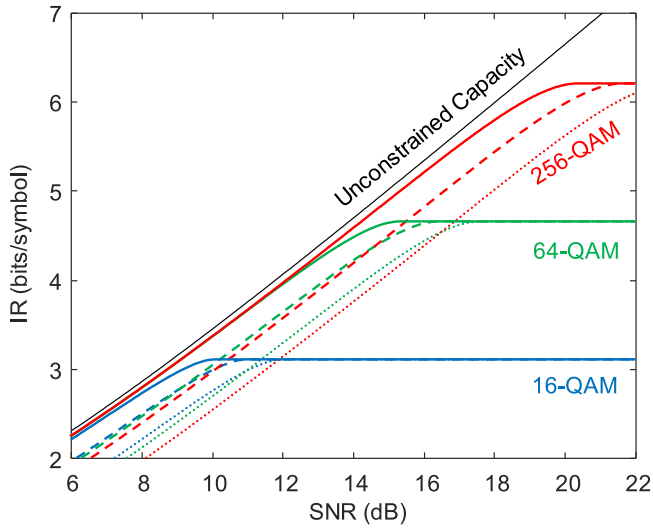

Fig. 15. IR of non-ideal PCS with $\delta_s = 0.025$, and non-ideal FEC with $\delta_c = 0$ (solid lines), $\delta_c = 0.05$ (dashed lines), and $\delta_c = 0.10$ (dotted lines).

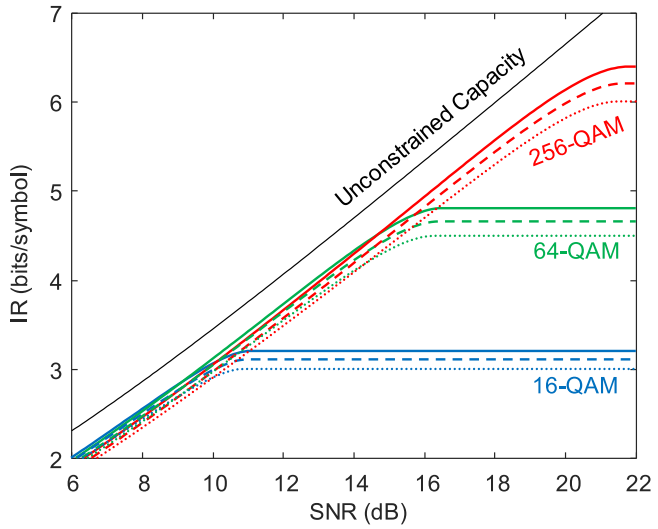

Fig. 16. IR of non-ideal FEC with $\delta_c = 0.05$, and non-ideal PCS with $\delta_s = 0$ (solid lines), $\delta_s = 0.025$ (dashed lines), and $\delta_s = 0.05$ (dotted lines).

V. Implementation Aspects

A. Distribution Matching

CCDM [56] is one of the most commonly assumed DMs for PCS in optical communications, since *(i)* it is asymptotically optimal in block length, simplifying the analysis of experimental results, and *(ii)* it can be implemented on the same architecture for any shaping rate. However, CCDM uses modified arithmetic coding that involves multiplications, divisions, and comparisons of real numbers. An approximate implementation of CCDM using fixed-point operations still needs multiplications and divisions of (possibly large) integer numbers, see, e.g., [90]; the effect of limited numerical precision on the performance can be analyzed following [91]. Furthermore, and more fundamentally, arithmetic coding is *intrinsically serial* in each block, and the block size should be large to approach capacity, which impedes parallel ASIC implementations.

Approaches to design a DM algorithm that is computationally efficient and also good for parallelization include PCDM, which was used in early demonstrations of PCS in optical communications [36]. This scheme is implemented using small look-up tables (LUTs), and a framing method for PCDM is presented in [58], [59], which allows variable-length prefix-free codes to be contained in a fixed-length block. Without framing, PCDM approaches the optimal energy efficiency to within a few tenths of a dB across a wide range of shaping rates with very fine granularity. Even after framing, the shaping gap is kept to within a few tenths of a dB if the block length is large. Like CCDM, PCDM is also an asymptotically good algorithm in block length. Indeed, the asymptotically good performance of CCDM and PCDM is intrinsic, since they are both designed to avoid the exponential complexity associated with the direct mapping of uniformly distributed information bits to an n_s-dimensional ball of constellation points, by generating IID MB distributions in large dimensions. Conversely, though, both schemes can result in a significant shaping gap for short block lengths.

However, for short block lengths (i.e., small dimensions $n_s \leq 100$), it is feasible by today's implementation technology to perform direct mapping of information bits to an n_s -dimensional ball-like constellation in an algorithmic manner, e.g., using *shell mapping* [63], [74]–[76]. Shell mapping was adopted in dial-up and fax modems in the mid-1990s, as defined in the ITU-T Standard V.34 [7]. Obviously, the shaping performance of shell mapping is somewhat sub-optimal due to its limited block length.

B. SD FEC

In BMD, the SD decoding metric of the j-th bit level can be represented by an LLR as (cf. (10))

$$L_j(y) = \log \frac{P_{B_j|Y}(0|y)}{P_{B_j|Y}(1|y)} = \log \frac{\sum_{x\in\mathcal{X}_0^{(j)}} P_{Y|X}(y|x) P_X(x)}{\sum_{x\in\mathcal{X}_1^{(j)}} P_{Y|X}(y|x) P_X(x)}. \quad (23)$$

When symbol X is uniformly distributed over $\mathcal{X}$, the LLR reduces to

$$L_j(y) = \log \frac{\sum_{x\in\mathcal{X}_0^{(j)}} P_{Y|X}(y|x)}{\sum_{x\in\mathcal{X}_1^{(j)}} P_{Y|X}(y|x)}$$

and an efficient piecewise-linear approximation of L_j [92] leads to near-optimal decoding performance in belief-propagation decoding of LDPC codes [93]. If we use PS QAM with an MB distribution P_X in an AWGN channel with noise variance σ^2, the LLR L_j can be calculated from the received signal y as

$$L_j(y) = \log \frac{\sum_{x\in\mathcal{X}_0^{(j)}} \exp\left(-\frac{(y-x)^2}{2\sigma^2} - \lambda x^2\right)}{\sum_{x\in\mathcal{X}_1^{(j)}} \exp\left(-\frac{(y-x)^2}{2\sigma^2} - \lambda x^2\right)}. \quad (24)$$

Let us denote the symbols that have a dominant effect in decoding as

$$x_0 = \underset{x\in\mathcal{X}_0^{(j)}}{\operatorname{argmax}} \exp\left(-\frac{(y-x)^2}{2\sigma^2} - \lambda x^2\right)$$

and

$$x_1 = \underset{x\in\mathcal{X}_1^{(j)}}{\operatorname{argmax}} \exp\left(-\frac{(y-x)^2}{2\sigma^2} - \lambda x^2\right),$$

respectively, from the numerator and the denominator of (24). Then, the max-log approximation of (24) using x_0 and x_1 leads to an LLR estimate of the j-th bit level, which is a linear function of y as

$$\tilde{L}_j(y) = \underbrace{\frac{x_0 - x_1}{\sigma^2} y}_{(a)} - \underbrace{\left(\frac{1}{2\sigma^2} + \lambda\right)\left(x_0^2 - x_1^2\right)}_{(b)}. \quad (25)$$

The term (a) is a function of the channel parameter σ, and the term (b) is a joint function of the channel (σ) and shaping (λ). When PS QAM degenerates to uniform QAM by $\lambda = 0$, (25) reduces to the conventional linear LLR approximation of uniform QAM, $L_j(y) = (x_0 - x_1)/\sigma^2 \times (y - (x_0 + x_1)/2)$. Figure 17 shows the exact and piecewise-linear approximate LLRs of the first 3 bit levels (i.e., of one quadrature) of a PS 64-QAM constellation with BRGC [101, 100, 110, 111, 011, 010, 000, 001].

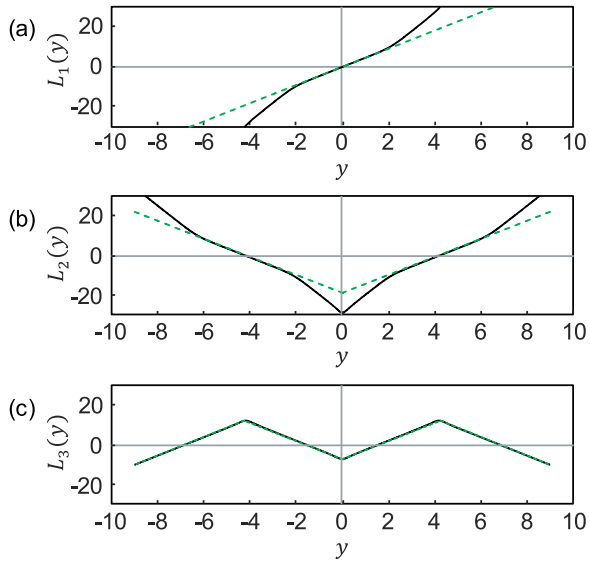

Fig. 17. Exact (solid lines) and piecewise-linear approximate (dashed lines) LLRs of the (a) first, (b) second, and (c) third bit levels, with $\mathbb{H}(X) = 2.6$ on the 64-QAM template at SNR $= 13$ dB.

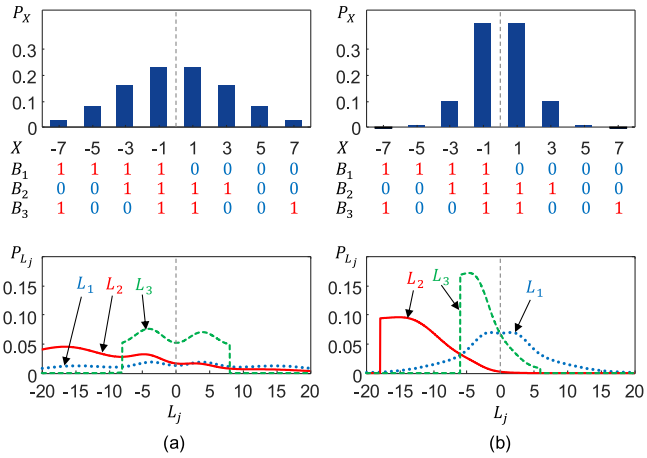

Fig. 18. Probabilities of 8-PAM constellation points X and LLRs L_j with (a) $\mathbb{H}(X) = 2.7$ at SNR $= 12.9$ dB, and (b) $\mathbb{H}(X) = 1.8$ at SNR $= 5.1$ dB.

The piecewise-linear approximation (dashed) yields LLRs that are indistinguishable from the exact (solid) LLRs when their magnitudes (i.e., the absolute values $|\tilde{L}_j(y)|$ on the y-axis) are small; i.e., the approximation error is negligible for those LLRs that play a crucial role in SD decoding. The approximation leads to an increasing discrepancy as the magnitude grows. This, however, has an insignificant impact on decoding performance, and almost no impact at high SNR.

SD FEC codes are typically designed by assuming symmetric LLR distributions, which occur, e.g., as a consequence of BICM with uniform QAM constellations. However, when a constellation is strongly shaped such that its shaping rate R_s is much smaller than $2m$, LLRs can have highly asymmetric distributions. Therefore, performance loss can be observed in pragmatic FEC decoding if the constellation is strongly shaped. As an example, the probability distribution of input symbol, $P_X(X)$, and that of the LLR, $P_{L_i}(L_i)$, are evaluated for two shaping rates $R_s = 2\mathbb{H}(X)$ with $\mathbb{H}(X) = 2.7$ and 1.8 in Fig. 18, using the 64-QAM template, $m = 3$, and the BRGC [101, 100, 110, 111, 011, 010, 000, 001] in each dimension. The LLR distributions are obtained at SNRs of 12.9 dB and 5.1 dB, respectively, which are the SNRs that achieve capacity with $R_s^* = 2\mathbb{H}(X)$. With weak shaping of $\mathbb{H}(X) = 2.7$, all LLR distributions are symmetric or close to symmetric. With strong shaping of $\mathbb{H}(X) = 1.8$, however, L_2 and L_3 become highly asymmetric around zero. In particular, at the second bit level, $P(L_2 < 0) \approx 0.9963$ and $P(L_2 > 0) \approx 0.0037$, hence the hard decision (HD) value of the demapper output is almost always bit 1. This results in the effect that the code bits are *nearly shortened* at the second bit level, which amounts to $1/3$ of the code bits. In the extreme case where $\lambda \to \infty$, hence $\mathbb{H}(X) = 1$, only the innermost constellation points have a non-zero probability of occurrence, which results in complete shortening of the code bits that are mapped to outer symbols (i.e., the code bits at the second and third bit levels in this example). Therefore, in order to support strong shaping, FEC codes should be designed to be robust to shortening at the bit levels with a highly asymmetric LLR distribution. With this, and looking back at the fact that a fixed coding gap causes a loss of IR that increases with m, overly strong shaping of a large QAM template, such as used, e.g., in [94], should be avoided for pragmatic FEC decoding. Instead, one should switch to a smaller QAM template whenever the shaping gap becomes small enough with weak shaping.

C. Pre-FEC Performance Metrics and HD FEC

In terms of reporting raw transmission performance (pre-FEC BER or Q-factors), attention has to be paid to how these are determined for a shaped constellation. When performing HD of the received symbols according to the maximum a posteriori (MAP) decision rule, the decoder chooses $\hat{x} = \underset{x \in \mathcal{X}}{\operatorname{argmax}} P_{X|Y}(x|y)$. If we represent the constellation symbols X in a binary form $\boldsymbol{B} = [B_1 \dots B_m]$ using the BRGC, two nearest-neighbor symbols $x_L, x_R \in \mathcal{X}$ of a received symbol y differ in only one bit. Denote this bit level by j. Then, the MAP decision can be made as $\hat{x} = \underset{x \in \{x_L, x_R\}}{\operatorname{argmax}} P_{B_j|Y}(b_j(x)|y)$. In other words, $\hat{x} = x_L$ if $P_{B_j|Y}(b_j(x_L)|y) > P_{B_j|Y}(b_j(x_R)|y)$, and $\hat{x} = x_R$ otherwise. Therefore, an optimal decision boundary is given by the value d such that $P_{B_j|Y}(b_j(x_L)|d) = P_{B_j|Y}(b_j(x_R)|d)$. That is, $P_{B_j|Y}(b_j(x_L)|d)/P_{B_j|Y}(b_j(x_R)|d) = 1$, hence $L_j(d) = 0$ (cf. (23)). The HD boundaries are a union of the HD boundaries of constituent bit levels. Since evaluation of exact $L_j(y)$ is complicated as shown in (24), and by knowing that the piecewise-linear approximate of LLR is very accurate in low-magnitude regimes (near $L_j(y) = 0$), we can obtain the HD boundaries using (25) as by $\tilde{L}_j(\tilde{d}) = 0$. Therefore, from (25), the union of HD boundaries of all bit levels is given by

$$\tilde{d}_k = \left(1 + 2\lambda\sigma^2\right) \frac{x_k + x_{k+1}}{2}, \tag{26}$$

for the M-PAM constellation $\mathcal{X} = [x_1, \dots, x_M]$ with $x_1 < \dots < x_M$. Notice that the boundary $\tilde{d}_k$ is a joint function of

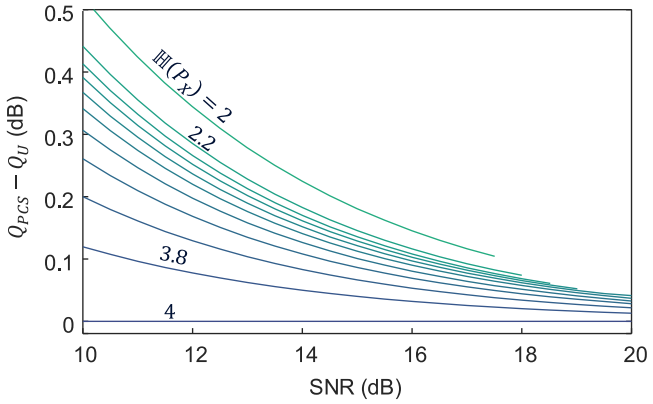

Fig. 19. Penalty in Q factor when the HD boundaries of uniform 16-QAM are used for PS 16-QAM.

the channel (σ) and shaping (λ). For uniform PAM with $\lambda = 0$, the boundaries in (26) reduce to $\tilde{d}_k = (x_k + x_{k+1})/2$, which is independent of the parameters σ and λ. Interestingly, given σ and λ, the PS PAM boundaries are simply a constant multiplication of the uniform PAM boundaries, hence making a uniform grid; e.g., if $\mathcal{D}_U = [\tilde{d}_1, \ldots, \tilde{d}_{M-1}] = [-6, -4, \ldots, +6]$ for uniform 8-PAM, $\mathcal{D}_{PCS} = [-6\Delta, -4\Delta, \ldots, +6\Delta]$ for PS 8-PAM, where $\Delta = 1 + 2\lambda\sigma^2$. Therefore, when PCS is used, the raw pre-FEC BER should be calculated based on $\mathcal{D}_{PCS}$ instead of $\mathcal{D}_U$. Figure 19 shows that, when PCS is performed, $Q_U = 10\log_{10}\text{BER}$ obtained with the uniform 16-QAM boundaries $\mathcal{D}_U$ can lead to > 0.5 dB of loss compared to Q_{PCS} obtained with the optimal PS 16-QAM boundaries $\mathcal{D}_{PCS}$.

VI. Conclusion

In this paper, we reviewed the theoretic foundation of PCS and discussed the merits of PCS over other constellation shaping techniques. Information-theoretic measures such as MI, GMI, and NGMI were explained with their operational meanings. Based on these measures, optimization problems are formulated for systems with optimal and sub-optimal PCS/FEC schemes, the solution of which provides the parameters of PCS and FEC that achieve the maximum IR under a given channel condition. We revisited important assumptions that are commonly made for ideal PCS and FEC systems, and addressed the potential pitfalls that should be avoided in practice.

Appendix

In this section, we show that $Q_{Y|X}(Y|X)$ in (11) represents an approximated channel transition probability that derives the GMI, in analogy to $P_{Y|X}(Y|X)$ that derives the MI, and its operational meaning is illustrated.

When binary codes are used with non-binary signaling, the multi-level coding and multi-stage decoding (MLC-MSD) [95], illustrated in Fig. 13(c), can achieve the SMD capacity. The MLC-MSD encodes each bit level using a different binary FEC code whose rate is matched to the bit level, and decodes the received symbols in a successive manner from the 1st constituent bit level to the m-th bit level, where each of the m decoders uses the (error-free) output of all the preceding decoders (cf. Fig. 13(c)). The reason why MLC-MSD can achieve the SMD capacity will become clear below.

First, recall that $\boldsymbol{B}$ is merely a binary representation of the non-binary symbol X, hence we have

$$P_{Y|X}\left(Y|X\right) = P_{Y|\boldsymbol{B}}\left(Y|\boldsymbol{B}\right) = \frac{P_{\boldsymbol{B}|Y}\left(\boldsymbol{B}|Y\right)P_Y\left(Y\right)}{P_{\boldsymbol{B}}(\boldsymbol{B})}, \quad (27)$$

where the last equation is again due to Bayes' rule. Here, using the chain rule, the likelihood can be rewritten as

$$\begin{aligned} P_{\boldsymbol{B}|Y}\left(\boldsymbol{B}|Y\right) &= P_{B_1\ldots B_m|Y}\left(B_1\ldots B_m|Y\right) \\ &= P_{B_1|Y}\left(B_1|Y\right) \times P_{B_2|B_1Y}\left(B_2|B_1Y\right)\cdots \\ &\quad \times P_{B_m|B_1\ldots B_{m-1}Y}\left(B_m|B_1\ldots B_{m-1}Y\right) \\ &= \prod_{j=1}^{m} P_{B_j|B_1\ldots B_{j-1}Y}(B_j|B_1\ldots B_{j-1}Y). \end{aligned} \quad (28)$$

For example, with the BRGC {101, 100, 110, 111, 011, 010, 000, 001} of the 8-PAM constellation $\mathcal{X} = -7, -5, \ldots, +7$, we have $\mathcal{X}_{00}^{(1,2)} \triangleq \{x \in \mathcal{X} : b_1(x) = 0,\ b_2(x) = 0\} = \{+5, +7\}$, hence $P_{Y|B_1B_2}(y|00) = \sum_{x' \in \mathcal{X}_{00}^{(1,2)}} P_{Y|X}(y|x')$ is calculated using the measurable $P_{Y|X}(Y|X)$, which in turn can be plugged into $P_{B_2|B_1Y}(0|0y) = P_{Y|B_1B_2}(y|00)\, P_{B_2}(0)/P_Y(y)$ to evaluate (28). Eventually, by plugging (28) into (27), we obtain an equivalent form of $P_{Y|X}(Y|X)$ expressed using the metrics of BMD as

$$\begin{aligned} &P_{Y|X}\left(Y|X\right) \\ &\quad = \left[\prod_{j=1}^{m} P_{B_j|B_1\ldots B_{j-1}Y}\left(B_j|B_1\ldots B_{j-1}Y\right)\right]\frac{P_Y\left(Y\right)}{P_X\left(X\right)}. \end{aligned} \quad (29)$$

Using (29), an optimal MLC-MSD that consists of m different length-n binary FEC codes finds m codewords $\boldsymbol{b}_1, \ldots, \boldsymbol{b}_m$ such that the product of the channel transition probabilities

$$\prod_{i=1}^{n}\Bigg[\underbrace{\prod_{j=1}^{m} P_{B_{i,j}|B_{i,1}\ldots B_{i,j-1}Y}\left(b_{i,j}|b_{i,1},\ldots,b_{i,j-1},y_i\right)}_{(a)}\Bigg]\underbrace{\frac{P_Y\left(y_i\right)}{P_X\left(x_i\right)}}_{(b)} \quad (30)$$

is maximized, where $b_{i,j}$ denotes the j-th bit of the transmitted symbol x_i. When $n_c \to \infty$, the terms (a) and (b) can be factored out of the product as $\lim_{n_c\to\infty}\prod_{i=1}^{n_c}[(a)(b)] = \lim_{n\to\infty}\prod_{i=1}^{n_c}(a)\cdot\lim_{n\to\infty}\prod_{i=1}^{n_c}(b)$, since both limits separately exist. In particular, due to the asymptotic equipartition property (AEP), $\prod_{i=1}^{n_c}(b)$ becomes concentrated at a fixed value $2^{-n_c(\mathbb{H}(Y)-\mathbb{H}(X))}$ that is independent of the choice of the codeword (i.e., independent of decoding), as $n_c \to \infty$. Therefore, decoding in MLC-MSD is a function only of the remaining term $\prod_{i=1}^{n_c}(a)$. The chain operations in (a) describe the successive decoding procedure of the MLC-MSD depicted in Fig. 13(c). This shows why

MLC-MSD can achieve the SMD capacity using binary codes and successive BMD.

MLC-MSD has a high complexity due to the use of multiple different FEC codes and a long latency due to successive decoding of bit levels and is hence not very practical. The parallel BMD architecture shown in Fig. 13(d) is a low-complexity low-latency alternative to MLC-MSD. Parallel BMD uses an approximation of the term (a) in (30) without relying on knowledge of any other bit levels as

$$P_{B_j|B_1,\ldots,B_{j-1},Y}(B_j\,|B_1,\ldots,B_{j-1},Y)\approx P_{B_j|Y}(B_j|Y). \quad (31)$$

By plugging the right-hand side of (31) into (29), it follows that the channel transition probability $P_{Y|X}(Y|X)$ can be approximated as (11), in which the term $P_Y(Y)/P_X(X)$ has a vanishing effect on decoding as the code length increases, for the same reason as in (30). Therefore, optimal BMD finds a codeword that maximizes the product of $P_{B_j|Y}(B_j|Y)$ over the received symbols that span all of the n_c codeword bits. Note that the mismatched decoding metric in (11) is valid for arbitrary distributions P_X, whereas the mismatched decoding metric has been derived for uniform P_X in most cases. In a special case where P_X is uniform and bit levels $B_1,\ldots,B_m$ are independent of each other, such as in BICM with BRGC, the mismatched decoding metric can be simplified as $Q_{Y|X}(Y|X)=\prod_{j=1}^{m} q_{Y|B_j}(Y|B_j)$, where $q_{Y|B_j}\triangleq\sum_{x'\in\mathcal{X}^i_{b_j(x)}} P_{Y|X}(Y|x')$, as derived in [87].

We are now to derive (13). First, by substituting (11) into (12), we have

$$\begin{aligned}
&GMI\,(X;Y)\\
&=\mathbb{E}_{X,Y}\left[\log_2\frac{Q_{Y|X}\,(Y\,|X\,)}{\sum_{x'\in\mathcal{X}}P_X\,(x')\,Q_{Y|X}\,(Y\,|x')}\right]\\
&=\sum_{x\in\mathcal{X}}\int_y P_{X,Y}\,(x,y)\log_2\frac{Q_{Y|X}\,(Y\,|X\,)}{\sum_{x'\in\mathcal{X}}P_X\,(x')\,Q_{Y|X}\,(Y\,|x')}dy\\
&=\sum_{x\in\mathcal{X}}\int_y P_{X,Y}(x,y)\log_2\frac{\prod_{j=1}^{m}P_{B_j|Y}\,(b_j\,(x)\,|y\,)}{P_X(x)\sum_{x'\in\mathcal{X}}\prod_{j=1}^{m}P_{B_j|Y}(b_j(x')\,|y\,)}dy\\
&=\sum_{x\in\mathcal{X}}\int_y P_{X,Y}(x,y)\log_2\frac{\prod_{j=1}^{m}P_{B_j|Y}\,(b_j\,(x)\,|y\,)}{P_X(x)\sum_{x'\in\mathcal{X}}\prod_{j=1}^{m}\frac{P_{B_jY}\,(b_j(x'),y)}{P_Y\,(y)}}dy\\
&=\sum_{x\in\mathcal{X}}\int_y P_{X,Y}\,(x,y)\\
&\quad\times\log_2\frac{\prod_{j=1}^{m}P_{B_j|Y}\,(b_j\,(x)\,|y\,)}{\frac{P_X\,(x)}{P_Y\,(y)^m}\sum_{x'\in\mathcal{X}}\prod_{j=1}^{m}P_{B_jY}\,(b_j\,(x')\,,y)}\,dy. \qquad (32)
\end{aligned}$$

In the denominator of the log term,

$$\begin{aligned}
&\sum_{x'\in\mathcal{X}}\prod_{j=1}^{m}P_{B_jY}\,(b_j\,(x')\,,y)\\
&\quad=\sum_{[b_1\ldots b_m\,]\in\{0,1\}^m}\prod_{j=1}^{m}P_{B_jY}\,(b_j,y)\\
&\quad=\sum_{[b_2\ldots b_m\,]\in\{0,1\}^{m-1}}P_{B_1Y}\,(0,y)\prod_{j=2}^{m}P_{B_jY}\,(b_j,y)\\
&\qquad+\sum_{[b_2\ldots b_m\,]\in\{0,1\}^{m-1}}P_{B_1Y}\,(1,y)\prod_{j=2}^{m}P_{B_jY}\,(b_j,y)\\
&\quad=(P_{B_1Y}(0,y)+P_{B_1Y}\,(1,y))\sum_{[b_2\ldots b_m\,]\in\{0,1\}^{m-1}}\prod_{j=2}^{m}P_{B_jY}(b_j,y)\\
&\quad=P_Y\,(y)\sum_{[b_2\ldots b_m\,]\in\{0,1\}^{m-1}}\prod_{j=2}^{m}P_{B_jY}\,(b_j,y)\,.
\end{aligned}$$

By recursion, therefore, we obtain

$$\sum_{x'\in\mathcal{X}}\prod_{j=1}^{m}P_{B_jY}\,(b_j\,(x')\,,y)=P_Y(y)^m\,.$$

By substituting this into (31), we have

$$\begin{aligned}
&GMI\,(X;Y)\\
&\quad=\sum_{x\in\mathcal{X}}\int_y P_{X,Y}\,(x,y)\log_2\frac{\prod_{j=1}^{m}P_{B_j|Y}\,(b_j\,(x)\,|y\,)}{P_X\,(x)}\,dy\\
&\quad=\underbrace{\sum_{x\in\mathcal{X}}\int_y\left[P_{X,Y}\,(x,y)\log_2\prod_{j=1}^{m}P_{B_j|Y}\,(b_j\,(x)\,|y\,)\right]dy}_{(a)}\\
&\qquad\underbrace{-\sum_{x\in\mathcal{X}}\int_y\left[P_{X,Y}\,(x,y)\log_2 P_X\,(x)\right]dy}_{(b)}\,.
\end{aligned}$$

The term (a) can be developed as

$$\begin{aligned}
(a)\;&=\sum_{x\in\mathcal{X}}\int_y\left[P_{X,Y}\,(x,y)\sum_{j=1}^{m}\log_2 P_{B_j|Y}\,(b_j\,(x)\,|y\,)\right]dy\\
&=\sum_{j=1}^{m}\int_y\left[\sum_{x\in\mathcal{X}}P_{X,Y}\,(x,y)\log_2 P_{B_j|Y}\,(b_j\,(x)\,|y\,)\right]dy\\
&=-\sum_{j=1}^{m}\mathbb{H}\,(B_j\,|Y\,)\,.
\end{aligned}$$

The term (b) can be developed as

$$\begin{aligned}
(b)\;&=-\sum_{x\in\mathcal{X}}\left[\int_y P_{X,Y}\,(x,y)\,dy\right]\log_2 P_X\,(x)\\
&=-\sum_{x\in\mathcal{X}}P_X\,(x)\log_2 P_X\,(x)\\
&=\mathbb{H}\,(X)\,.
\end{aligned}$$

Therefore, we obtain

$$GMI\,(X;Y)=(a)+(b)=\mathbb{H}\,(X)-\sum_{j=1}^{m}\mathbb{H}\,(B_j\,|Y\,)\,,$$

which is equal to (13).

REFERENCES

[1] C. E. Shannon, "A mathematical theory of communication," *Bell Syst. Tech. J.*, vol. 27, no. 3, pp. 379–423, Jul. 1948.

[2] G. D. Forney Jr., R. G. Gallager, G. R. Lang, F. M. Longstaff, and S. U. Qureshi, "Efficient modulation for band-limited channels," *IEEE J. Sel. Areas Commun.*, vol. SAC-2, no. 5, pp. 632–647, Sep. 1984.

[3] A. R. Calderbank and L. H. Ozarow, "Nonequiprobable signaling on the Gaussian channel," *IEEE Trans. Inf. Theory*, vol. 36, no. 4, pp. 726–740, Jul. 1990.

[4] G. D. Forney Jr., "Trellis shaping," *IEEE Trans. Inf. Theory*, vol. 38, no. 2, pp. 281–300, Mar. 1992.

[5] F. R. Kschischang and S. Pasupathy, "Optimal nonuniform signaling for Gaussian channels," *IEEE Trans. Inf. Theory*, vol. 39, no. 3, pp. 913–929, May 1993.

[6] F.-W. Sun and H. C. A. van Tilborg, "Approaching capacity by equiprobable signaling on the Gaussian channel," *IEEE Trans. Inf. Theory*, vol. 39, no. 5, pp. 1714–1716, Sep. 1993.

[7] A Modem Operating at Data Signalling Rates of Up to 33 600 Bit/S for Use On the General Switched Telephone Network and On Leased Point-To-Point 2-Wire Telephone-Type Circuits, ITU-T Recommendation V.34, Feb. 1998.

[8] C. Berrou, A. Glavieux, and P. Thitimajshima, "Near Shannon limit error-correcting coding and decoding: Turbo-codes. 1," in *Proc. IEEE Int. Conf. Commun.*, Geneva, Switzerland, May 1993, vol. 2, pp. 1064–1070.

[9] R. Gallager, "Low-density parity-check codes," *IRE Trans. Inf. Theory*, vol. 8, no. 1, pp. 21–28, Jan. 1962.

[10] D. J. C. MacKay and R. M. Neal, "Near Shannon limit performance of low density parity check codes," *Electron. Lett.*, vol. 32, no. 18, pp. 1645–1646, Aug. 1996.

[11] T. J. Richardson, M. A. Shokrollahi, and R. L. Urbanke, "Design of capacity-approaching irregular low-density parity-check codes," *IEEE Trans. Inf. Theory*, vol. 47, no. 2, pp. 619–637, Feb. 2001.

[12] Unified high-speed wireline-based home networking transceivers – System architecture and physical layer specification, ITU-T Recommendation G.9960, Jul. 2015.

[13] IEEE Standard for Ethernet, IEEE Std 802.3, Sep. 2015.

[14] Part 11: Wireless LAN Medium Access Control (MAC) and Physical Layer (PHY) Specifications, IEEE Std 802.11, Dec. 2016.

[15] IEEE Standard for Air Interface for Broadband Wireless Access Systems, IEEE Std 802.16, Aug. 2012.

[16] Second Generation Framing Structure, Channel Coding and Modulation Systems for Broadcasting, Interactive Services, News Gathering and Other Broadband Satellite Applications; Part 1 (DVB-S2), ETSI EN 302 307-1, Nov. 2014.

[17] A. Leven and L. Schmalen, "Status and recent advances on forward error correction technologies for lightwave systems," *J. Lightw. Technol.*, vol. 32, no. 16, pp. 2735–2750, Aug. 2014.

[18] G. Tzimpragos, C. Kachris, I. B. Djordjevic, M. Cvijetic, D. Soudris, and I. Tomkos, "A survey on FEC codes for 100 G and beyond optical networks," *IEEE Commun. Surv. Tut.*, vol. 18, no. 1, pp. 209–221, Jan.–Mar. 2016.

[19] L. Duan, B. Rimoldi, and R. Urbanke, "Approaching the AWGN channel capacity without active shaping," in *Proc. IEEE Int. Symp. Inf. Theory*, Jun. 1997, p. 374.

[20] D. Raphaeli and A. Gurevitz, "Constellation shaping for pragmatic turbo-coded modulation with high spectral efficiency," *IEEE Trans. Commun.*, vol. 52, no. 3, pp. 341–345, Mar. 2004.

[21] S. L. Goff, B. Sharif, and S. Jimaa, "Bit-interleaved turbo-coded modulation using shaping coding," *IEEE Commun. Lett.*, vol. 9, no. 3, pp. 246–248, Mar. 2005.

[22] F. Schreckenbach and P. Henkel, "Signal shaping using non-unique symbol mappings," in *Proc. Allerton Conf. Commun. Control Comput.*, Sep. 2005, pp. 1–10.

[23] B. K. Khoo, S. Le Goff, B. Sharif, and C. Tsimenidis, "Bit-interleaved coded modulation with iterative decoding using constellation shaping," *IEEE Trans. Commun.*, vol. 54, no. 9, pp. 1517–1520, Sep. 2006.

[24] S. Kaimalettu, A. Thangaraj, M. Bloch, and S. McLaughlin, "Constellation shaping using LDPC codes," in *Proc. IEEE Int. Symp. Inf. Theory*, Jun. 2007, pp. 2366–2370.

[25] H. Cronie, "Signal shaping for bit-interleaved coded modulation on the AWGN channel," *IEEE Trans. Commun.*, vol. 58, no. 12, pp. 3428–3435, Dec. 2010.

[26] R.-J. Essiambre, G. Kramer, P. J. Winzer, G. J. Foschini, and B. Goebel, "Capacity limits of optical fiber networks," *J. Lightw. Technol.*, vol. 28, no. 4, pp. 662–701, Feb. 2010.

[27] I. B. Djordjevic, H. G. Batshon, L. Xu, and T. Wang, "Coded polarization-multiplexed iterative polar modulation (PM-IPM) for beyond 400 Gb/s serial optical transmission," in *Proc. Opt. Fiber. Conf.*, San Diego, CA, USA, Mar. 2010, Paper OMK2.

[28] T. H. Lotz *et al.*, "Coded PDM-OFDM transmission with shaped 256-iterative-polar-modulation achieving 11.15-b/s/Hz intrachannel spectral efficiency and 800-km reach," *J. Lightw. Tehcnol.*, vol. 31, no. 4, pp. 538–545, Feb. 2013.

[29] J.-X. Cai *et al.*, "70.46 Tb/s over 7,600 km and 71.65 Tb/s over 6,970 km transmission in C+L band using coded modulation with hybrid constellation shaping and nonlinearity compensation," *J. Lightw. Tehcnol.*, vol. 36, no. 1, pp. 114–121, Jan. 2018.

[30] R. T. Jones, T. A. Eriksson, Y. P. Metodi, and D. Zibar, "Deep learning of geometric constellation shaping including fiber nonlinearities," in *Proc. Eur. Conf. Opt. Commun.*, Rome, Italy, Sep. 2018, Paper We1F.5.

[31] R. Dar, M. Feder, A. Mecozzi, and M. Shtaif, "Properties of nonlinear noise in long, dispersion-uncompensated fiber links," *Opt. Express*, vol. 21, no. 22, pp. 25685–25699, Nov. 2013.

[32] T. Fehenberger, A. Alvarado, G. Böcherer, and N. Hanik. "On probabilistic shaping of quadrature amplitude modulation for the nonlinear fiber channel," *J. Lightw. Technol.*, vol. 34, no. 21, pp. 5063–5073, Nov. 2016.

[33] G. Böcherer, F. Steiner, and P. Schulte., "Bandwidth efficient and rate-matched low-density parity-check coded modulation," *IEEE Trans. Commun.*, vol. 63, no. 12, pp. 4651–4665, Dec. 2015.

[34] T. Fehenberger, G. Bocherer, A. Alvarado, and N. Hanik, "LDPC coded modulation with probabilistic shaping for optical fiber systems," in *Proc. Opt. Fiber Commun. Conf.*, Los Angeles, CA, USA, Mar. 2015, Paper Th.2.A.23.

[35] F. Buchali, G. Bocherer, W. Idler, L. Schmalen, P. Schulte, and F. Steiner, "Experimental demonstration of capacity increase and rate-adaptation by probabilistically shaped 64-QAM," in *Proc. Eur. Conf. Opt. Commun.*, Valencia, Spain, Sep. 2015, Paper PDP.3.4.

[36] S. Chandrasekhar *et al.*, "High-spectral-efficiency transmission of PDM 256-QAM with parallel probabilistic shaping at record rate-reach tradeoffs," in *Proc. Eur. Conf. Opt. Commun.*, Dusseldorf, Germany, Sep. 2016, Paper Th.3.C.1.

[37] A. Ghazisaeidi *et al.*, "65 Tb/s transoceanic transmission using probabilistically-shaped PDM-64QAM," in *Proc. Eur. Conf. Opt. Commun.*, Dusseldorf, Germany, Sep. 2016, Paper Th.3.C.4.

[38] J. Cho *et al.*, "Trans-Atlantic field trial using high spectral efficiency probabilistically shaped 64-QAM and single-carrier real-time 250-Gb/s 16-QAM," *J. Lightw. Technol.*, vol. 36, no. 1, pp. 103–113, Jan. 2018.

[39] S. L. I. Olsson, J. Cho, S. Chandrasekhar, X. Chen, P. J. Winzer, and S. Makovejs, "Probabilistically shaped PDM 4096-QAM transmission over up to 200 km of fiber using standard intradyne detection," *Opt. Express*, vol. 26, no. 4, pp. 4522–4530, Feb. 2018.

[40] S. L. I. Olsson, J. Cho, S. Chandrasekhar, X. Chen, E. C. Burrows, and P. J. Winzer, "Record-high 17.3-bit/s/Hz spectral efficiency transmission over 50 km using probabilistically shaped PDM 4096-QAM," in *Proc. Opt. Fiber Commun. Conf.*, San Diego, CA, USA, Mar. 2018, Paper Th4C.5.

[41] Nokia Corporation, Nokia Photonic Service Engine 3. 2018. [Online]. Available: https://networks.nokia.com/photonic-service-engine-3

[42] J. Li *et al.*, "Field trial of probabilistic-shaping-programmable real-time 200-Gb/s coherent transceivers in an intelligent core optical network," in *Proc. Asia Commun. Photon. Conf.*, Hangzhou, China, Oct. 2018, Paper Su2C.1.

[43] G. Kramer, M. I. Yousefi, and F. R. Kschischang, "Upper bound on the capacity of a cascade of nonlinear and noisy channels," in *Proc. Inf. Theory Workshop*, Jerusalem, Israel, Apr. 2015, pp. 1–4.

[44] P. Poggiolini, G. Bosco, A. Carena, V. Curri, Y. Jiang, and F. Forghieri, "The GN-model of fiber non-linear propagation and its applications," *J. Lightw. Tehcnol.*, vol. 32, no. 4, pp. 694–721, Feb. 2014.

[45] R. Dar, M. Feder, A. Mecozzi, and M. Shtaif, "Accumulation of nonlinear interference noise in fiber-optic systems," *Opt. Express*, vol. 22, no. 12, pp. 14199–14211, May 2014.

[46] R. Dar, M. Shtaif, and M. Feder, "New bounds on the capacity of the nonlinear fiber-optic channel," *Opt. Lett.*, vol. 39, no. 2, pp. 398–401, Jan. 2014.

[47] S. Ten Brink, "Convergence behavior of iteratively decoded parallel concatenated codes," *IEEE Trans. Commun.*, vol. 49, no. 10, pp. 1727–1737, Oct. 2001.

[48] T. Tian and C. R. Jones, "Construction of rate-compatible LDPC codes utilizing information shortening and parity puncturing," *EURASIP J. Wireless Commun. Netw.*, vol. 2005, no. 5, pp. 789–795, Dec. 2005.

[49] T. V. Nguyen, A. Nosratinia, and D. Divsalar, "The design of rate-compatible protograph LDPC codes," *IEEE Trans. Commun.*, vol. 60, no. 10, pp. 2841–2850, Oct. 2012.

[50] D. G. M. Mitchell, M. Lentmaier, A. E. Pusane, and D. J. Costello, "Randomly punctured LDPC codes," *IEEE J. Sel. Areas Commun.*, vol. 34, no. 2, pp. 408–421, Feb. 2016.

[51] J. Ha, J. Kim, and S. McLaughlin, "Rate-compatible puncturing of low-density parity-check codes," *IEEE Trans. Inf. Theory*, vol. 50, no. 11, pp. 2824–2826, Nov. 2004.

[52] C.-H. Hsu and A. Anastasopoulos, "Capacity achieving LDPC codes through puncturing," *IEEE Trans. Inf. Theory*, vol. 54, no. 10, pp. 4698–4706, Oct. 2008.

[53] R. Asvadi and A. H. Banihashemi, "A rate-compatible puncturing scheme for finite-length LDPC codes," *IEEE Commun. Lett.*, vol. 17, no. 1, pp. 147–150, Jan. 2013.

[54] J. Cho, X. Chen, S. Chandrasekhar, and P. Winzer, "On line rates, information rates, and spectral efficiencies in probabilistically shaped QAM systems," *Opt. Express*, vol. 26, no. 8, pp. 9784–9791, Apr. 2018.

[55] J. Cho, "Balancing probabilistic shaping and forward error correction for optimal system performance," in *Proc. Opt. Fiber. Conf.*, San Diego, CA, USA, Mar. 2018, Paper M3C-2.

[56] P. Schulte and G. Böcherer, "Constant composition distribution matching," *IEEE Trans. Inf. Theory*, vol. 62, no. 1, pp. 430–434, Jan. 2016.

[57] J. Cho, S. Chandrasekhar, R. Dar, and P. J. Winzer, "Low-complexity shaping for enhanced nonlinearity tolerance," in *Proc. Eur. Conf. Opt. Commun.*, Dusseldorf, Germany, Sep. 2016, Paper W1C.2.

[58] J. Cho, "Prefix-free code distribution matching for probabilistic constellation shaping," *IEEE Trans. Commun.*, submitted for publication.

[59] J. Cho *et al.*, "Probabilistic signal shaping and codes therefor," U.S. Patent Appl. 15/374397, Dec. 9, 2016.

[60] G. Böcherer, F. Steiner, and P. Schulte, "Fast probabilistic shaping implementation for long-haul fiber-optic communication systems," in *Proc. Eur. Conf. Opt. Commun.*, Gothenburg, Sweden, Sep. 2017, Paper Tu.2.D.3.

[61] T. Yoshida, M. Karlsson, and E. Agrell, "Short-block-length shaping by simple mark ratio controllers for granular and wide-range spectral efficiencies," in *Proc. Eur. Conf. Opt. Commun.*, Gothenburg, Sweden, Sep. 2017, Paper Tu.2.D.2.

[62] T. Yoshida, M. Karlsson, and E. Agrell, "Low-complexity variable-length output distribution matching with periodical distribution uniformalization," in *Proc. Opt. Fiber. Conf.*, San Diego, CA, USA, Mar. 2018, Paper M4E.2.

[63] P. Schulte and F. Steiner, "Divergence-optimal fixed-to-fixed length distribution matching with shell mapping," *IEEE Wireless Commun. Lett.*, to be published.

[64] S.-Y. Chung, G. D. Forney, T. J. Richardson, and R. Urbanke, "On the design of low-density parity-check codes within 0.0045 dB of the Shannon limit," *IEEE Commun. Lett.*, vol. 5, no. 2, pp. 58–60, Feb. 2001.

[65] W.-R. Peng, I. Morita, and H. Tanaka, "Hybrid QAM transmission techniques for single-carrier ultra-dense WDM systems," in *Proc. Opto-Electron. Commun. Conf.*, Kaohsiung, Taiwan, Jul. 2011, pp. 824–825.

[66] X. Zhou *et al.*, "4000 km transmission of 50 GHz spaced, 10×494.85-Gb/s hybrid 32-64QAM using cascaded equalization and training-assisted phase recovery," in *Proc. Opt. Fiber. Conf.*, Los Angeles, CA, USA, Mar. 2012, Paper PDP5C.6.

[67] M. Xiang *et al.*, "Multi-subcarrier flexible bit-loading enabled capacity improvement in meshed optical networks with cascaded ROADMs," *Opt. Express*, vol. 25, no. 21, pp. 25046–25058, Oct. 2017.

[68] F. P. Guiomar, L. Bertignono, A. Nespola, and A. Carena, "Frequency-domain hybrid modulation formats for high bit-rate flexibility and nonlinear robustness," *J. Lightw. Technol.*, vol. 36, no. 20, pp. 4856–4870, Oct. 2018.

[69] J. Cho, S. Chandrasekhar, X. Chen, G. Raybon, and P. J. Winzer, "High spectral efficiency transmission with probabilistic shaping," in *Proc. Eur. Conf. Opt. Commun.*, Gothenburg, Sweden, Sep. 2017, Paper Th.1.E.1.

[70] G. D. Forney, *Principles of Digital Communication II*. Cambridge, MA, USA: MIT OpenCourseWare, Sep. 7, 2018. [Online]. Available: https://ocw.mit.edu

[71] T. M. Cover and J. A. Thomas, *Elements of Information Theory*, 2nd ed. Hoboken, NJ, USA: Wiley, 2006.

[72] S. Arimoto, "An algorithm for computing the capacity of arbitrary discrete memoryless channels," *IEEE Trans. Inf. Theory*, vol. 18, no. 1, pp. 14–20, Jan. 1972.

[73] R. Blahut, "Computation of channel capacity and rate-distortion functions," *IEEE Trans. Inf. Theory*, vol. 18, no. 4, pp. 460–473, Jul. 1972.

[74] G. R. Lang and F. M. Longstaff, "A Leech lattice modem," *IEEE J. Sel. Areas Commun.*, vol. 7, no. 6, pp. 968–973, Aug. 1989.

[75] A. K. Khandani and P. Kabal, "Shaping multidimensional signal spaces. I. Optimum shaping, shell mapping," *IEEE Trans. Inf. Theory*, vol. 39, no. 6, pp. 1799–1808, Nov. 1993.

[76] R. Laroia, N. Farvardin, and S. A. Tretter, "On optimal shaping of multidimensional constellations," *IEEE Trans. Inf. Theory*, vol. 40, no. 4, pp. 1044–1056, Jul. 1994.

[77] H. D. Pfister, J. B. Soriaga, and P. H. Siegel, "On the achievable information rates of finite state ISI channels," in *Proc. IEEE GlobeCom*, San Antonio, TX, USA, Nov. 2001, pp. 2992–2996.

[78] J. Cho, S. Chandrasekhar, and P. Winzer, "Rate-adaptive modulation schemes for high spectral efficiency optical communications," in *Proc. OSA Frontiers Opt.*, Washington, DC, USA, Sep. 2018, Paper FW5B-1.

[79] A. Alvarado, E. Agrell, D. Lavery, R. Maher, and P. Bayvel, "Replacing the soft-decision FEC limit paradigm in the design of optical communication systems," *J. Lightw. Technol.*, vol. 33, no. 20, pp. 4338–4352, Oct. 2015.

[80] J. Cho, L. Schmalen, and P. Winzer, "Normalized generalized mutual information as a forward error correction threshold for probabilistically shaped QAM," in *Proc. Eur. Conf. Opt. Commun.*, Gothenburg, Sweden, Sep. 2017, Paper M.2.D.2.

[81] A. Alvarado, T. Fehenberger, B. Chen, and F. M. J. Willems, "Achievable information rates for fiber optics: Applications and computations," *J. Lightw. Technol.*, vol. 36, no. 2, pp. 424–439, Jan. 2018.

[82] G. Böcherer, "Achievable rates for probabilistic shaping," 2018, arXiv:1707.01134.

[83] G. Böcherer, "On joint design of probabilistic shaping and FEC for optical systems," in *Proc. Opt. Fiber Conf.*, San Diego, CA, USA, Mar. 2018, Paper M4E-1.

[84] G. Böcherer, P. Schulte, and F. Steiner, "Probabilistic shaping and forward error correction for fiber-optic communication systems," *J. Lightw. Technol.*, to be published.

[85] T. Yoshida, M. Karlsson, and E. Agrell, "Performance metrics for systems with soft-decision FEC and probabilistic shaping," *IEEE Photon. Technol. Lett.*, vol. 29, no. 23, pp. 2111–2114, Dec. 2017.

[86] N. Merhav, G. Kaplan, A. Lapidoth, and S. Shamai Shitz, "On information rates for mismatched decoders," *IEEE Trans. Inf. Theory*, vol. 40, no. 6, pp. 1953–1967, Nov. 1994.

[87] A. Martinez, A. G. i Fàbregas, G. Caire, and F. M. J. Willems, "Bit-interleaved coded modulation revisited: A mismatched decoding perspective," *IEEE Trans. Inf. Theory*, vol. 55, no. 6, pp. 2756–2765, Jun. 2009.

[88] J. Cho, S. L. I. Olsson, S. Chandrasekhar, and P. Winzer, "Information rate of probabilistically shaped QAM with non-ideal forward error correction," in *Proc. Eur. Conf. Opt. Commun.*, Rome, Italy, Sep. 2018, Paper Th1H.5.

[89] J. Cho and P. J. Winzer, "Multi-rate prefix-free code distribution matching," in *Proc. Opt. Fiber Commun. Conf.*, to be published.

[90] G. Böcherer, F. Steiner, and P. Schulte, "Fast probabilistic shaping implementation for long-haul fiber-optic communication systems," in *Proc. Eur. Conf. Opt. Commun.*, Gothenburg, Sweden, Sep. 2017, Paper Tu.2.D.3.

[91] T. V. Ramabadran, "A coding scheme for m-out-of-n codes," *IEEE Trans. Commun.*, vol. 38, no. 8, pp. 1156–1163, Aug. 1990.

[92] F. Tosato and P. Bisaglia, "Simplified soft-output demapper for binary interleaved COFDM with application to HIPERLAN/2," in *Proc. Int. Conf. Commun.*, New York, NY, USA, May 2002, vol. 2, pp. 664–668.

[93] G. Baruffa and L. Rugini, "Soft-output demapper with approximated LLR for DVB-T2 systems," in *Proc. IEEE GlobeCom*, San Diego, CA, USA, Dec. 2015, pp. 1–6.

[94] R. Maher, K. Croussore, M. Lauermann, R. Going, X. Xu, and J. Rahn, "Constellation shaped 66 GBd DP-1024QAM transceiver with 400 km transmission over standard SMF," in *Proc. Eur. Conf. Opt. Commun.*, Gothenburg, Sweden, Sep. 2017, Paper Th.PDP.B.2.

[95] H. Imai and S. Hirakawa, "A new multilevel coding method using error-correcting codes," *IEEE Trans. Inf. Theory*, vol. 23, no. 3, pp. 371–377, May 1977.

Junho Cho (M'10) received the B.S., M.S., and Ph.D. degrees in electrical engineering and computer science from Seoul National University, Seoul, South Korea. He has been with Bell Labs, Seoul, South Korea from 2010 to 2014, and with Holmdel, NJ, USA since 2014. He was a Ph.D. dissertation committee member for Seoul National University. He has authored or coauthored numerous papers and serves as a reviewer for a wide range of IEEE journals, the scope of which includes the optics, communications, circuits and systems, and computer. His current research interests are probabilistic constellation shaping, forward error correction, and signal processing. He was the recipient of the Outstanding Research Award under the Brain Korea 21 Project while studying with Seoul National University in 2009.

Peter J. Winzer (F'09) received the Ph.D. degree from the Vienna University of Technology, Vienna, Austria, where he worked on space-borne lidar and laser communications for the European Space Agency. Since 2000, he has been with Bell Labs, Holmdel, NJ, USA, and has focused on many aspects of fiber-optic communications and networking, from advanced optical modulation, multiplexing, and detection to cross-layer network architectures. He has contributed to several high-speed optical transmission records from 100 Gb/s to 1 Tb/s in laboratory experiments and field trials, and has been widely promoting spatial multiplexing to overcome the optical networks capacity crunch. He has amply authored or coauthored and patented, and is actively involved with the IEEE Photonics Society and the Optical Society of America, including service as the Program Chair of ECOC 2009, Program/General Chair of OFC 2015/17, and the former Editor-in-Chief for the IEEE/OSA JOURNAL OF LIGHTWAVE TECHNOLOGY. He was the recipient of multiple awards for his work and is a highly cited researcher. He is a Fellow of Bell Labs and the OSA, and an elected member of the U.S. National Academy of Engineering.